DEPARTMENT OF ELECTRONIC & ELECTRICAL ENGINEERING

University of Strathclyde Engineering

University of Strathclyde

Wind Energy & Control

Control of aeroelastically-tailored wind turbines

Luis Recalde-Camacho

Adam Stock

Alexander Duncan Giles

supervised by

Prof. William Leithead

January 24, 2020

Contents

List of Figures

1 Summary

This document reports on reduction of wind turbine fatigue loads on multi-MW wind turbines with passive adaptive strategies or by reducing rotor weight.

Passive adaptive structural load alleviation is achieved by combining well-tuned speed controllers, with load alleviation capabilities, and new adaptive blade configurations developed by project partners at the University of Bristol. New types of composite material, whose properties vary spatially both along and across the blade, are used to produce two adaptive, aero-elastically tailored blade configurations named material adaptive and combined adaptive. Material bend-twist coupling is induced by anisotropic composite materials, whereas combined coupling is induced by embedding anisotropy and using a curved, swept blade planform to produce additional geometric bend-twist coupling. The two aero-elastic blade configurations are used in the NREL 5 MW wind turbine rotor and compared against the NREL 5 MW baseline rotor. Drive-train viscous losses are added to the electrical loses to make all three wind turbines as similar as possible and allow a fair performance comparison. Controllers are designed in frequency domain and their structure and parameters are also kept similar when possible for the three the wind turbines. Power production simulations are carried out to assess fatigue loading over the operating wind speed range (4 m/s to 24 m/s). An extreme gust simulation scenario is also tested.

A control system is also designed for the light weight rotor DTU 10 MW wind turbine. The DTU 10 MW wind turbine was designed at the Technical University of Denmark (DTU) in their HAWC 5 software tool and converted into a Bladed model by project partners at the University of Bristol. The DTU 10 MW turbine has a light weight rotor developed by increasing the thickness to chord ratio of airfoils along the blade span and adjusting the thickness of the load carrying structural elements in the blade such that the blade twist passively adapts to changes in the wind field, and weight and edgewise loads scale better with flapwise loads while considering the negative impact from higher thickness ratio on power and thrust. Fatigue loads are also assessed for this wind turbine exemplar.

2 Introduction

2.1 Bend-twist coupling

Research and development of bend-twist coupling in wind turbine applications is not a new area of research. In 1992, Garrad Hassan published a report commenting on the occurrence of wind turbines with bend-twist coupling [CM92]. Several companies were listed as having implemented some form of passive power control in their designs: Lagerwey, NPS, Berewould, Flexhat, Swedewind and Carter. Of these, it would appear that only Lagerwey, NPS and Carter still exist.

Lagerwey is the only company from the aforementioned companies that sell MW-scale wind turbines; in addition, no other company from the above list (that is still in existence) employs pitch control apart from Lagerwey; that is, all other existing companies use stall regulation. Lagerwey builds most components in-house, but, critically, this does not cover the blades. The only information that can be found on the blades used by Lagerwey is that they are glass-fibre reinforced polyester.

NPS currently market four wind turbines. All are variable-speed stall-regulated. While the company may have ventured into aero-elastically tailored blades in the past, there is no definitive indication that any of the currently marketed wind turbines employ aero-elastically tailored

blades. If aero-elastically tailored blades were still in use, it would be reasonable to assume that the structure is designed to induce a nose-up response that increases in wind speed, which would drive the blade into stall, which is consistent with the control approach (stall regulation).

Carter's brochures mention a unique flexible composite blade design that enables the blade to twist in order to change the angle of attack along the length of the blade.

Around the turn of the millennium, Lobitz & Veers studied aero-elastically tailored blades for horizontal axis wind turbines [LVL99][LVE$^+$01]. In contrast to the turbines discussed in the preceding paragraphs, where the turbines use torsional flexibility to promote the occurrence of stall, the blade design presented is one which the blade has structural properties to induce a rotation towards feather (nose-down) of the blade sections. By having a blade pitch passively towards feather, the angle of attack is reduced and with it the forces to which the blade is subjected. It was shown that significant load reductions could be achieved without causing unacceptable energy capture degradation. In [LV03], the same authors investigated the combined effects of control strategy and bend-twist coupling on turbine performance. For variable-speed pitch-controlled rotors, it is shown that twist coupling facilitates a substantial decrease in fatigue damage over all turbulent wind fields simulated without compromising average power levels. It is concluded that *whenever a rotor is operating in the linear aerodynamic range, substantial reductions in fatigue damage are realised* [LV03]. For the studies involving bend-twist coupled blades with pitch control, an adaptive control scheme is developed in K. Pierce [LV03]. However, no further details are provided. The term adaptive is fairly vague, since many control schemes can be described as adaptive. Presumably, in order to avoid hunting issues, the pitch controller would have to be atypical. Whatever control system is adopted, results indicate that the transition from below-rated to above-rated wind speeds (where the pitch control becomes active) is sub-optimal, with a small degradation, or bump, being visible in the power curve around rated wind speed. The fact that this occurs in both results for the twist-coupled rotor and the uncoupled rotor suggests that the switching algorithm in the controller is where attention should be paid [1].

Locke et al. also studied bend-twist coupled rotors in [LH02][LVI03]. The choice of material was the principal focus of this research. Carbon fibres were applied. More recently, research has been conducted at the University of Bristol, [CPW14, CPW15, SCL$^+$17a], on aeroelastic tailoring to induce a nose-down twist response or twist towards feather, as such response promotes load alleviation in variable-speed pitch regulated wind turbines.

2.2 Implications of bend-twist coupling on control design

The power and torque developed by a wind turbine can be inferred from a simple steady state BEM analysis and are expressed as follows:

$$P = \frac{1}{2}\rho\pi R^2 C_{\mathrm{p}}(\lambda,\beta)v^3 \tag{1}$$

$$T = \frac{1}{2}\rho\pi R^3 C_{\mathrm{q}}(\lambda,\beta)v^2 \tag{2}$$

$$\lambda = \frac{R\Omega_{\mathrm{R}}}{v} \tag{3}$$

$$C_{\mathrm{q}} = \frac{C_{\mathrm{p}}}{\lambda} \tag{4}$$

[1] It is possible to achieve smooth switching with a non twist-coupled rotor, which suggests that, if the controller is solely responsible for the bump, it may be possible to realise smooth switching on a twist-coupled rotor also.

where ρ is the density of the air ($\rho = 1.225$), C_p and C_q are the wind turbine power and torque coefficients, λ is the tip speed ratio, R is the rotor radius, v is the wind speed and Ω_R is the rotor speed.

Generally speaking, the generated power of a typical wind turbine with non-tailored blades depends on the total twist distribution of the blade that is the sum of the pitch angle $\beta_\mathrm{ctrl}(v)$ produced by the pitch controller and the pre-twist distribution, $\gamma(r)$, which is a function of the radial position, r, [CPW14]. The annual energy production (AEP) can therefore be maximised by choosing the blade pre-twist to be optimal at a given wind speed and tracking a suitable control strategy across the operating envelope. An operating strategy in the torque/rotor speed plane can be split into regions, as seen in Figure 1. The variables ω_0 and ω_1 are the minimum and maximum limits of the rotor speed operating range; and T_0 and T_1 are minimum and maximum aerodynamic torques when operating the wind turbine on the maximum power tracking region. Rotor speed ω_1 is also the rated rotor speed and T_{set} is the rated torque. At the first constant speed region, rotor speed is regulated to ω_0, in closed-loop, until the torque reaches T_0. At the second constant speed region, rotor speed is regulated to ω_1 until the aerodynamic torque reaches its rated value, T_{set}. When the wind turbine reaches its rated values, nonlinear aerodynamics are compensated with gain-scheduling and rotor speed is regulated by acting on the pitch angle, either collectively or individually on the blades. Regulation is maintained until a maximum wind speed is reached (cut-off wind speed) at which the wind turbine has to be shut-down for security reasons.

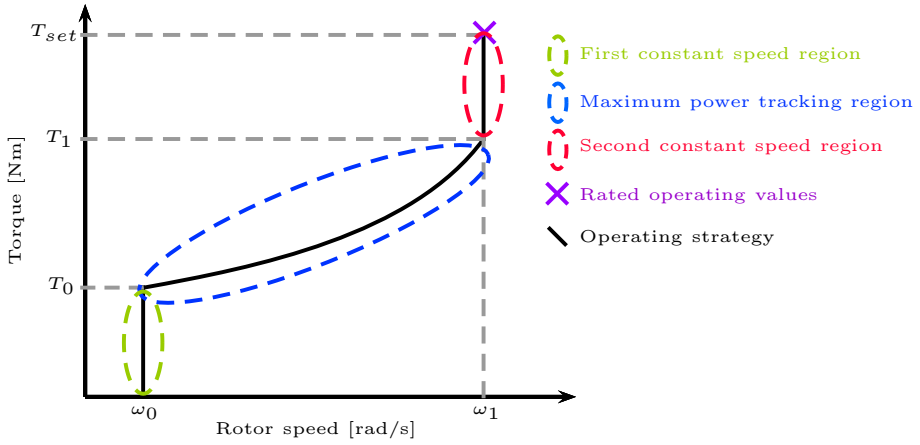

Figure 1: Typical operating control strategy for a variable speed wind turbine

At the maximum power tracking region, the wind turbine is operated at its optimum power efficiency. For non-tailored blades, this is achieved by tracking the optimimum power coefficient, $C_{p_\mathrm{max}}(\lambda^*, \beta_0)$ with $\beta_0 \cong 0$. Optimal tip speed ratio, λ^*, is the only design parameter and needs to be chosen carefully by considering issues such as power efficiency, shaft torque, torque and blade structural stiffness. Non-tailored blades are torsionally rigid thus there is only one, widely-accessible λ^* at which aerodynamic efficiency has a global maxima. The generator torque demand is calculated as follows:

$$T_G = K_\mathrm{opt}\Omega_G^2 \tag{5}$$

where the gain $K_\mathrm{opt} = \frac{1}{2}\rho\pi R^5 \frac{C_{p\mathrm{max}}(\lambda^*,0)}{\lambda^* N^3}$ is the optimal controller gain.

Tailored blades configurations, on the other hand, are torsionally soft due to bend-twist coupling embedded into the blade. The induced twist contribution, $\zeta(r, \Omega_\mathrm{R}, v)$, is a function of wind speed, radial position and rotor speed, thus making the aerodynamic profile of the blade

torsionally flexible as wind speed changes. The total twist distribution becomes

$$\zeta_{\text{total}} = \zeta(r, \Omega_{\text{R}}, v) + \gamma(r) + \beta_{\text{ctrl}}(v) \tag{6}$$

The adaptive blade configurations used in this report have been optimised at rated wind speed values, using single-objective optimisation, to obtain the total twist distributions that maximise AEP. For consistency, the baseline blade static-twist distributions are also optimised, see [SCL$^+$17a]. For any other wind speeds, particularly at below rated values, induced twist deflections may make aerodynamic efficiency radially dependent. The single global maxima still exists at a specific rated speed, however the value of λ^* is no longer constant and the wind turbine can only operate at near optimum power efficiency. To control the turbine, a series of optimised K_{opt} values, along the maximum power tracking region, can be determined if the drive train efficiency is not altered, as presented in [SCL$^+$17a]. However in this report, to assess bent-twist coupling performance fairly, drive-train efficiency is modified and the rotors no longer operate at maximum aerodynamic efficiency, thus using a single local maxima λ^* to control the turbine suffixes.

The remainder of this report is structured as follows. Key features of each wind turbine exemplars are compared and their influence for control design is presented in Section 3. Control strategy and controller synthesis are developed to be as similar as possible for the three wind turbine exemplars and is presented in Section 4. Tower and drive-train fatigue loads are also minimised using a method called Power coordinated control and a drive-train damper, respectively. Simulations studies are carried out in Section 5. Power capture, generator speed regulation, gust operation and fatigue loads are assessed. Controller design and performance assessment for the 10 MW wind turbine exemplar is presented in Section 6. Conclusions are drawn in Section 7.

3 Wind turbine key features

The two aeroelastically-tailored blade configurations differ from the NREL 5 MW wind turbine in blade mass and rotor diameter as seen in Table 1. The mass increase in the material adaptive blade configuration is due to off-axis composite plies located in both the spar cap and skins to introduce bend-twist coupling [SCL$^+$17b]. Figure 2 shows the total twist distribution given by Equation 6. Material adaptive blade configuration shows a steep twist towards feather from root to tip whereas the combined adaptive blade configuration follows a steep increase from root to mid-span followed by a softer increase towards to tip. Both, material adaptive and combined adaptive blade configurations are able to achieve an increase in twist towards feather at the blade tip of 4.7° and 3.1°, respectively, at 12 m/s wind speed. Aeroelastic twist, pitch angle and pre-twist distributions, for 12 m/s wind speed, can be seen in Figures 3, 4 and 5. As reported in [SCL$^+$17a], pre-twist distributions have been adapted from the pre-twist distribution of the baseline model to achieve an optimal total twist distribution. Steady-state pitch angle has been slightly reduced and the major variation is found in the aeroelastic twist, particularly for the combined adaptive blade configuration which aeroelastic twist to feather increases significantly from root to mid-span and then decreases towards the tip, see Figure 3. Material adaptive

Table 1: Wind turbine features

Wind turbine	**Blade mass [kg]**	**Rotor diameter [m]**
Baseline	16762	126.267
Material adaptive	17138	126.267
Combined adaptive	16344	125.593

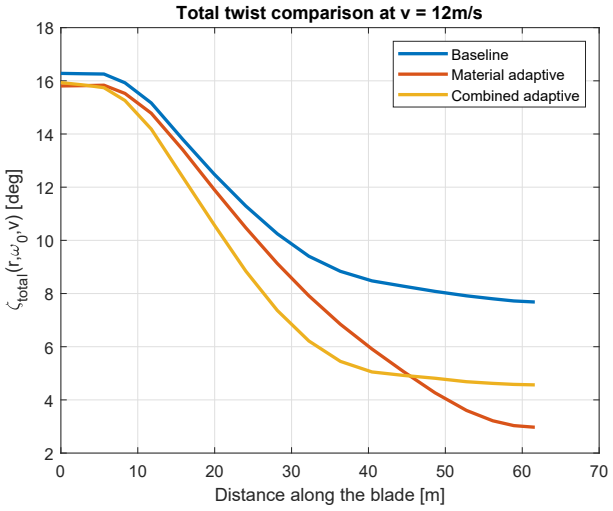

Figure 2: Total twist distribution at 12 m/s wind speed

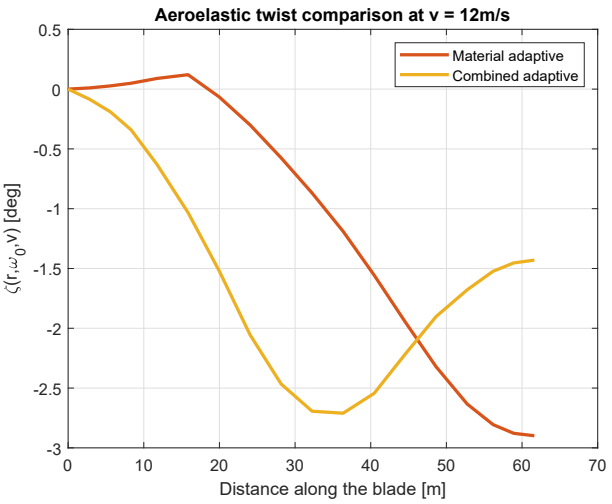

Figure 3: Induced aeroelastic twist at 12 m/s wind speed

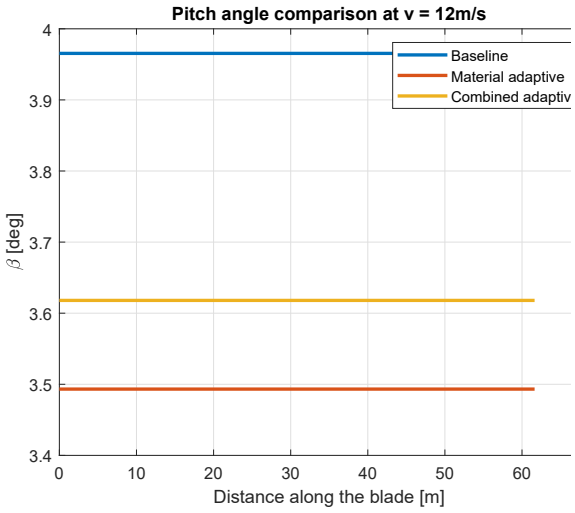

Figure 4: Pitch angle at 12 m/s wind speed

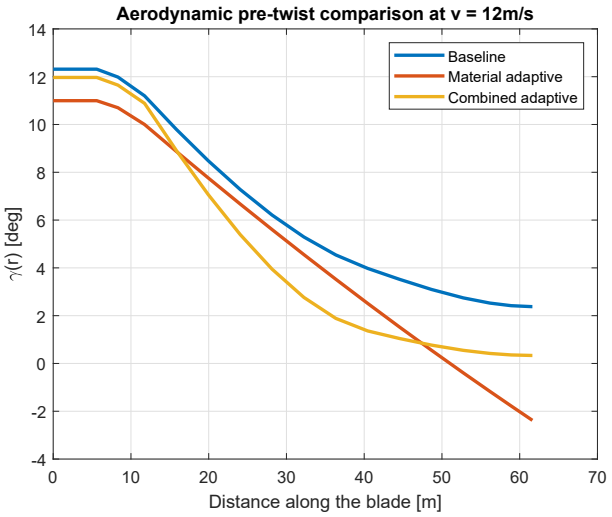

Figure 5: Pre-twist distribution at 12 m/s wind speed

and combined adaptive aeroelastic twist curves across the wind speed operating envelope can be seen in Figures 6 and 7, respectively. Both blade configurations reach peak twist towards feather at wind speed rated values. At below rated wind speed values, the aero-elastic twist increases as wind speed increases up to rated wind speed, thus underpinning the design strategy presented in [SCL+17a] when no drivetrain losses have been added. At above rated wind speed values the twist curves start to decrease because most of the total twist is exerted by the pitch system. At wind speeds up and above 22 m/s, the combined adaptive blade configuration starts to twist towards stall in the mid-span to match the tip twist of the material adaptive blade configuration as originally intended during blade design.

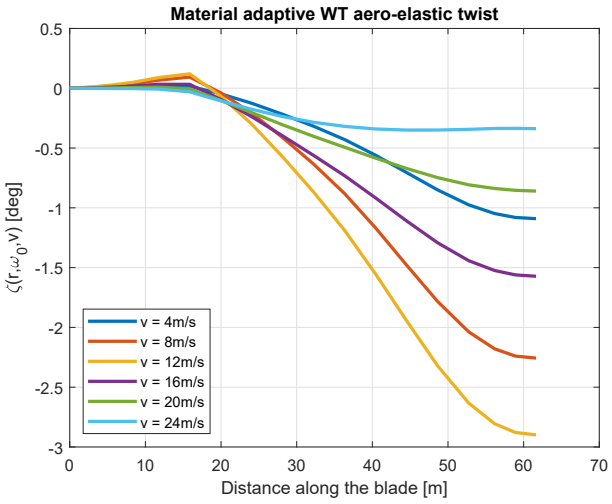

Figure 6: Material adaptive aero-elastic twist comparison

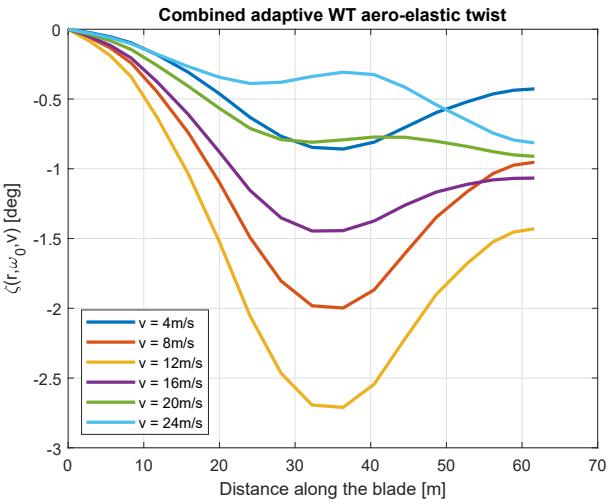

Figure 7: Combined adaptive aero-elastic twist comparison

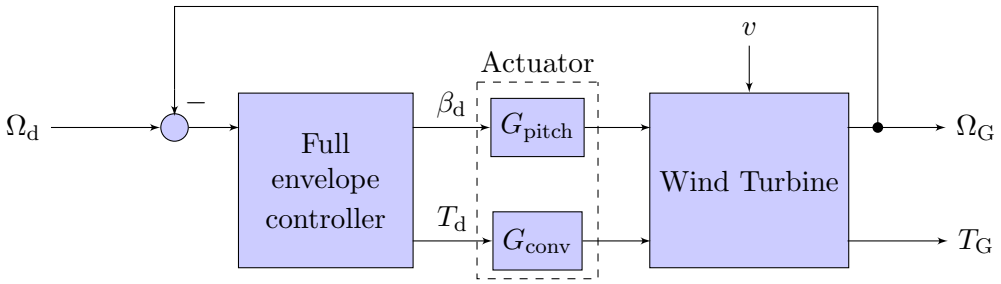

Figure 8: Wind turbine standard control system

4 Controller design

Full envelope controllers are designed to maintain the turbines operating states, i.e. rotor speed, generated power, aerodynamic torque, etc., at their wind speed-dependent design values (rated vales). Figure 8 shows the basic control system required for pitch regulated variable speed wind turbines. The wind turbine dynamics are non-linear and non-minimum phase. The non-linearity can be adequately catered for to obtain a simplified model which is essentially linear. The non-minimum phase phenomenon, caused by right half plane zeros, time delays and sampling effects, introduces a limitation on the achievable open-loop bandwidth and constrains the sensitivity characteristic of the close-loop for disturbance rejection and parameter variation [LC00]. The controller produces a variation in torque through a pitch actuator in above rated wind speeds and through a power converter in below rated wind speeds. The actuators are non-linear but can also be adequately approximated by linear models. The variations in wind speed can be considered as stochastic disturbances that the controller rejects over the operating envelope. The operating envelope, which is wind speed-dependent, can be expressed as a non-linear control strategy requiring a non-linear controller.

4.1 Control strategy

Ideally, for fair comparison between different rotors, the control strategy should be the same for all three rotors as should be rated rotor speed, rated power and power-train losses. Achieving all

these requirements is rather demanding but reasonable. For the three rotors used in this report, all power-train losses have been modelled as electrical losses having the same value of 90 %. This enables rated rotor speed and rated aerodynamic power to be kept the same at rated wind speed values of 11.6 m/s, 11.7 m/s and 11.6 m/s for the baseline model, material adaptive blade configuration and combined adaptive blade configuration, respectively. Nevertheless, there still remains significant differences in the wind speed range for the maximum power tracking region and the aerodynamic efficiencies.

Figure 9 shows the operating control strategy for the baseline model. The variables ω_0 and ω_1 are set to be 0.7233 rad/s and 1.2671 rad/s, T_0 and T_1 are reached at 6.1 m/s and 10.8 m/s, respectively. A drive-train efficiency of 90 % allows the second constant speed region to be large enough to guarantee controller stability during switching between below and above rated wind speed values. The achieved $C_{p_{\max}}$ is 0.4761 at $\lambda^* = 7.4$. Figures 10 and 11 show the operating strategies for material adaptive and combined adaptive blade configurations. Variables ω_0, ω_1 and drive-train efficiencies are kept the same as the baseline model. Material adaptive shows the longest second constant speed region with T_0 and T_1 being reached at 5.8 m/s and 10.3 m/s, respectively. Aerodynamic efficiency is slightly higher with 0.4768 $C_{p_{\max}}$ at $\lambda^* = 7.9$. The control strategy developed for the combined adaptive blade configuration is more similar to the one developed for the baseline model with T_0 and T_1 reached at 6 m/s and 10.7 m/s, respectively. Nonetheless, its aerodynamic efficiency is the highest of the three rotors with 0.48664 $C_{p_{\max}}$ at $\lambda^* = 7.6$. Figure 12 shows the aerodynamic power coefficients of the three wind turbines.

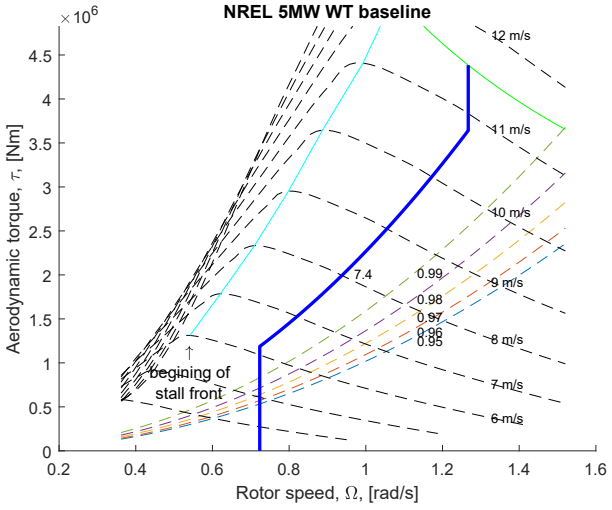

Figure 9: NREL 5 MW WT standard control strategy

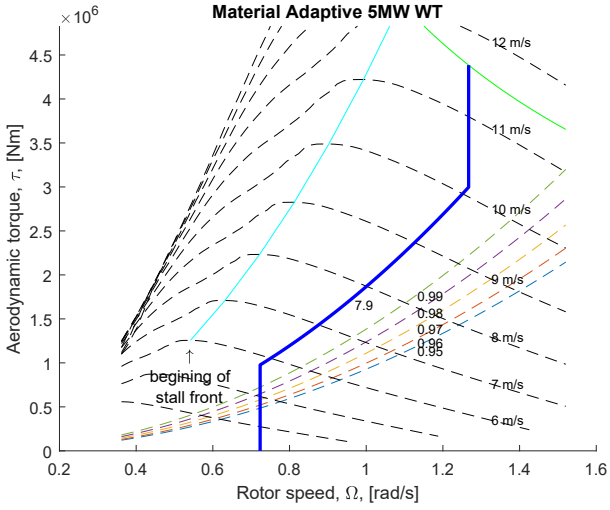

Figure 10: Material adaptive blade configuration control strategy

4.2 Controller synthesis

A non-linear control problem, such as the wind turbine control problem, requires a non-linear controller. A simple approach to the design of the controller would be to design a gain-scheduled-like controller. Gain-scheduling is non-linear feedback formed by a linear controller whose parameters and gain are changed as a function of the operating conditions in a pre-determined way. For each above rated wind speed value, the rated value of the aerodynamic torque is attained at a unique pitch angle and at rated rotor speed. These pitch angles, together with their corresponding wind speeds define the locus of equilibrium operating points (β, ω_0, v); that is, the aerodynamic torque at the rotor is non-linearly dependent on the blade pitch angle and

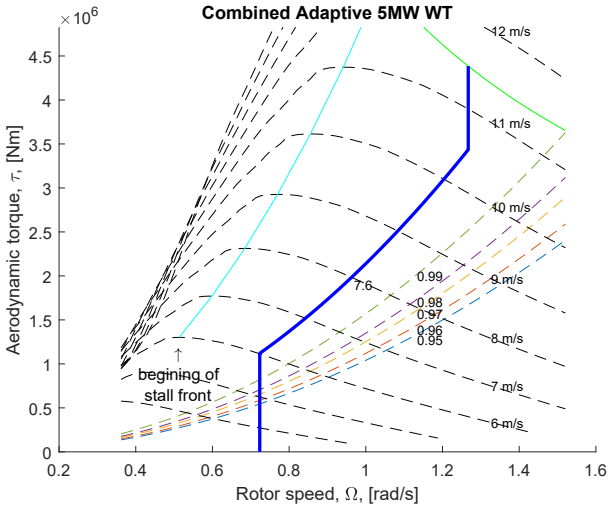

Figure 11: Combined adaptive blade configuration control strategy

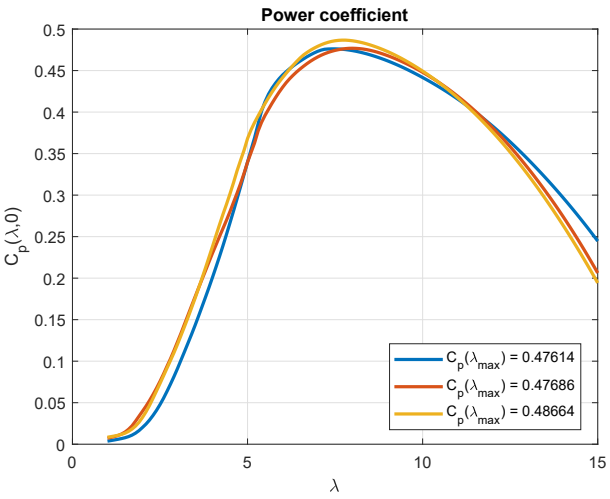

Figure 12: Aerodynamic power coefficient comparison

the wind speed. For conventional wind turbines, it is known that the aerodynamics can be reformulated as

$$T_f(\beta, \omega, v) \equiv \tau(\epsilon); \epsilon = h(\beta, \omega_0) - g(v) \tag{7}$$

over a neighbourhood sufficiently large to encompass all operating points, whether equilibrium or non-equilibrium, that are encountered during normal above rated operation. It follows that the dynamic relationship from pitch demand (β_d) to generator speed (Ω_G) can be represented as in Figure 13.

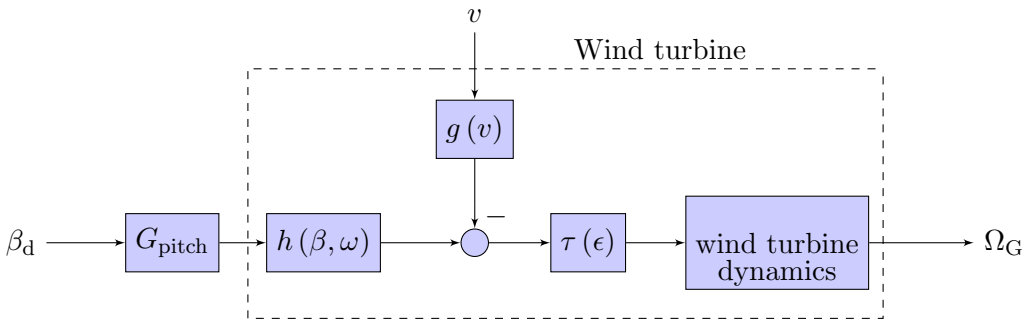

Figure 13: Equivalent wind turbine

Since the rotor speed is kept close to its rated value by the controller and its value does not vary rapidly, due to the inertia of the rotor, $h(\beta, \omega_0)$ is only weakly dependent on ω_0. Furthermore, τ is weakly dependent on ϵ. Hence, for control purposes the dynamics can be thought of as linear except for the input non-linearity $h(\beta, \omega_0)$ and linear controller design methods can be directly applied. A controller of this form, when linearised, has the appearance of a traditional gain-scheduled controller yet it is a global and not a local solution. The controller is designed in the frequency domain and assessed using Bode Diagrams. In linearised form, it contains the following components:

$$C(s) = -K_{\text{gs}}(\beta)\left[K_c \frac{N(s)}{sD(s)}\right] \tag{8}$$

- a lead compensator $\frac{N(s)}{D(s)}$ to cancel a low frequency pole, speed up system response and increase system stability;

- gain K_c that depends whether the turbine is operating at below or above rated wind speed;
- an integral action $\frac{1}{s}$ to ensure rejection of steady wind disturbances and suitable low frequency shaping to ensure rejection of gusts; and
- a gain $K(\beta)$ scheduled with the operating point to compensate the non-linear aerodynamic at above rated wind speeds i.e. to counteract $h(\beta, \omega_0)$.

From Equation 7, $K(\beta) = \left[\frac{\partial h(\beta,\omega)}{\partial \beta}|_{\omega_0}\right]^{-1}$, with $\frac{\partial h(\beta,\omega)}{\partial \beta}|_{\omega_0} = \frac{\partial T_f(\beta,\omega,v)}{\partial \beta}|_{\omega_0}$ and $\frac{\partial T_f(\beta,\omega,v)}{\partial \beta}|_{\omega_0}$ can be linearly approximated to

$$\frac{\partial T_f(\beta,\omega,v)}{\partial \beta}|_{\omega_0} \approx M\beta + C \tag{9}$$
$$K(\beta_{\text{rated}}) = 1$$

The variation of T_f with respect to β can be seen in Figure 14 for both adaptive blade con-

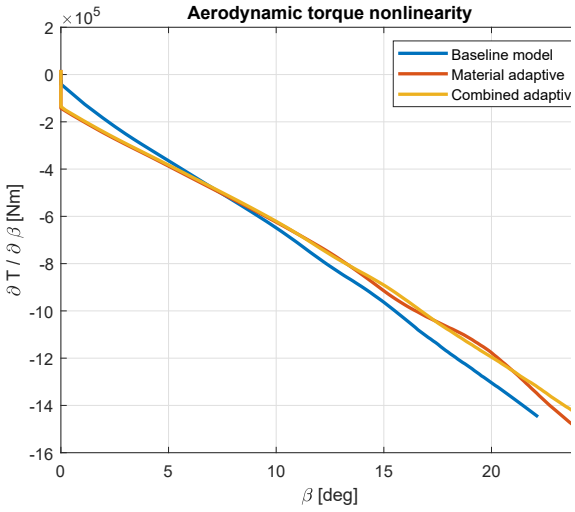

Figure 14: Aerodynamic torque nonlinearity

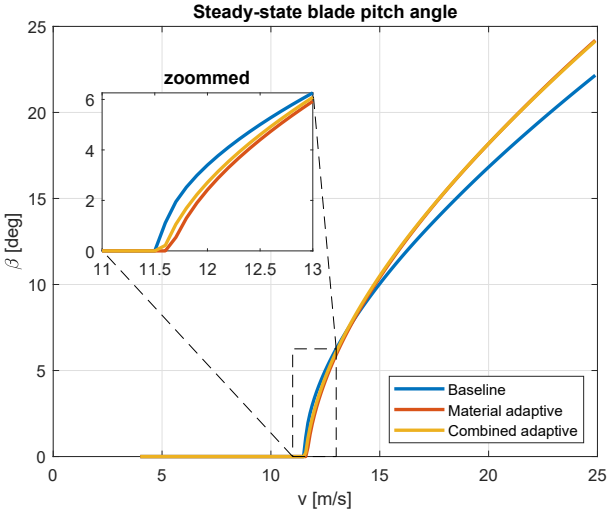

Figure 15: Comparison of steady-state pitch angle

figurations and the baseline model. The variation of $\frac{\partial T_f}{\partial \beta}$ at below rated values is larger on the blade adaptive configurations than on the baseline model due to the induced aero-elastic twist as seen in Figure 14. Nonetheless, it increases at a smaller rate to achieve similar values to those developed by the baseline model at higher wind speeds. The effect of the induced aero-elastic twist is also seen in Figure 15 where material adaptive blade configuration starts pitching at 11.7 m/s wind speed and even though the combined adaptive blade configuration starts pitching at 11.6 m/s, the required pitch angle is rather small. At higher wind speeds, the induced twist curve flattens up thus requiring higher pitch angles.

System damping and speed of the transient response can be indirectly assessed through gain "Gm" and phase "Pm" stability margins, and gain crossover frequency ω_{gco}, respectively. The controllers for the three wind turbines are designed with the same low frequency zero of 0.19. Controller gain and pole are used to achieve the same crossover frequency of 0.42 rad/s, both at below and above rated wind speeds. At above rated wind speeds, gain scheduling is set to keep the crossover frequency as similar as possible to the design value.

For the baseline model, the developed controllers are

$$C_{\mathrm{br}}^{\mathrm{B}}(s) = -\frac{4031.1\,(s+0.19)}{s\,(s+2.3)} \tag{10}$$

$$C_{\mathrm{ar}}^{\mathrm{B}}(s) = -\frac{0.014087\,(s+0.19)}{s\,(s+2.3)} \tag{11}$$

$$K_{\mathrm{gs}}^{\mathrm{B}}(\beta) = \frac{1}{0.1353\beta + 0.54} \tag{12}$$

$$K_{\mathrm{opt}}^{\mathrm{B}} = 2.4848 \tag{13}$$

C_{br} is the controller used in the first and second constant speed regions, K_{opt} is the optimal gain required to track the maximum power region. C_{ar} and K_{gs} are the above rated linear controller, designed at 14 m/s wind speed, and the scheduled gain, respectively. Note that both controllers have the same dynamics; however, the controller gains are rather different since C_{br} acts on torque whereas C_{ar} acts on blade pitch angle. Figure 16 shows the frequency analysis of the transmittance from pitch demand to generator speed for wind speeds of (12, 14, 16, 20) m/s wind speeds. Stability margins obtained with the frequency analysis are summarised in Table 2.

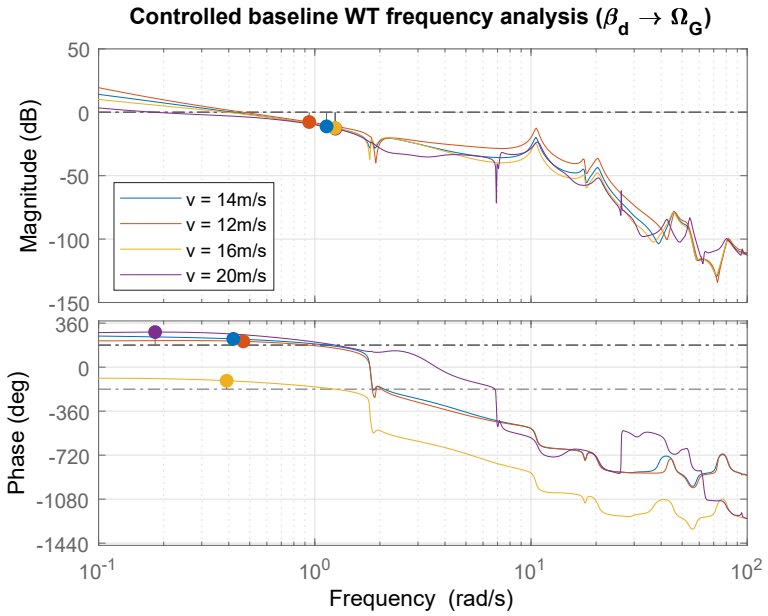

Figure 16: Baseline adaptive 5 MW controlled wind turbine frequency response

The developed controllers for the material adaptive blade configuration are

$$C_{\mathrm{br}}^{\mathrm{MA}}(s) = -\frac{3984.4\,(s+0.19)}{s\,(s+2.1)} \tag{14}$$

$$C_{\mathrm{ar}}^{\mathrm{MA}}(s) = -\frac{0.017513\,(s+0.19)}{s\,(s+2.1)} \tag{15}$$

$$K_{\mathrm{gs}}^{\mathrm{MA}}(\beta) = \frac{1}{0.1176\beta + 0.7156} \tag{16}$$

Table 2: Baseline 5 MW WT stability margins

v [m/s]	Gm [db]	Pm [deg]	Wpm [rad/s]	Delay Margin [s]
		Above rated controller		
12	7.67	31.1	0.467	1.16
14	11.1	51.3	**0.42**	2.13
16	12.3	69	0.391	3.08
20	12.9	107	0.183	10.2
		Below rated controller		
4	∞	56.1	**0.42**	2.33

$$K_{\text{opt}}^{\text{MA}} = 2.0453 \tag{17}$$

A pole at 2.1 and a higher controller gain is required to stabilise the rotor and achieve 0.42 rad/s gain crossover frequency. Frequency analysis and stability margins are presented in Figure 17 and Table 3, respectively. Gain-scheduling performs slightly better, particularly at 20 m/s wind speed.

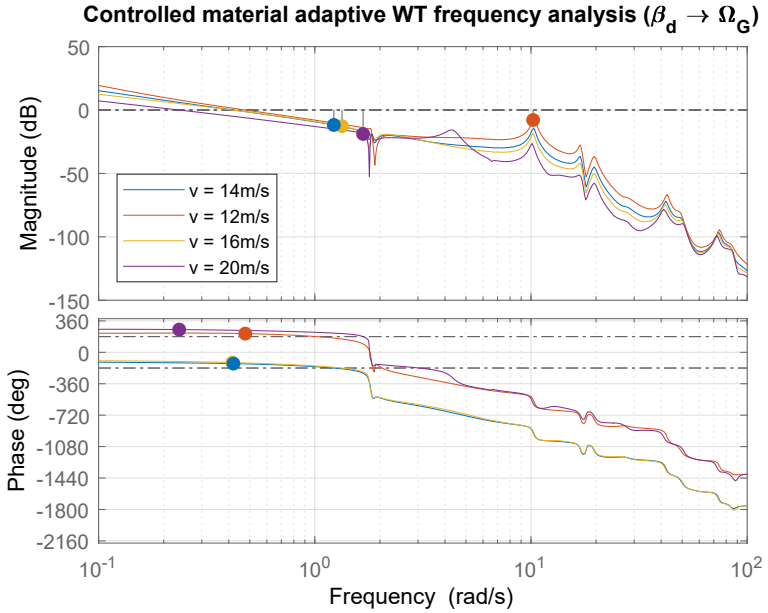

Figure 17: Material adaptive 5 MW controlled wind turbine frequency response

Table 3: Material adaptive 5 MW WT stability margins

v [m/s]	Gm [db]	Pm [deg]	Wpm [rad/s]	Delay margin [s]
		Above rated controller		
12	7.85	34.3	0.477	1.25
14	11.8	50.5	**0.42**	2.1
16	12.7	62.4	0.416	2.62
20	18.9	80.5	0.236	5.96
		Below rated controller		
4	∞	55	**0.42**	2.29

The controllers developed for the combined adaptive blade configuration are

$$C_{\mathrm{br}}^{\mathrm{CA}}(s) = -\frac{4109.3\,(s+0.19)}{s\,(s+2.2)} \tag{18}$$

$$C_{\mathrm{ar}}^{\mathrm{CA}}(s) = -\frac{0.017622\,(s+0.19)}{s\,(s+2.2)} \tag{19}$$

$$K_{\mathrm{gs}}^{\mathrm{CA}}(\beta) = \frac{1}{0.1120\beta + 0.6966} \tag{20}$$

$$K_{\mathrm{opt}}^{\mathrm{CA}} = 2.0453 \tag{21}$$

These controllers are fairly similar to the ones developed for the material adaptive blade configurations, but gain-scheduling performs a lot better achieving a crossover frequency of 0.356 rad/s at 20 m/s wind speed. Frequency analysis and stability margins are presented in Figure 18 and Table 4, respectively.

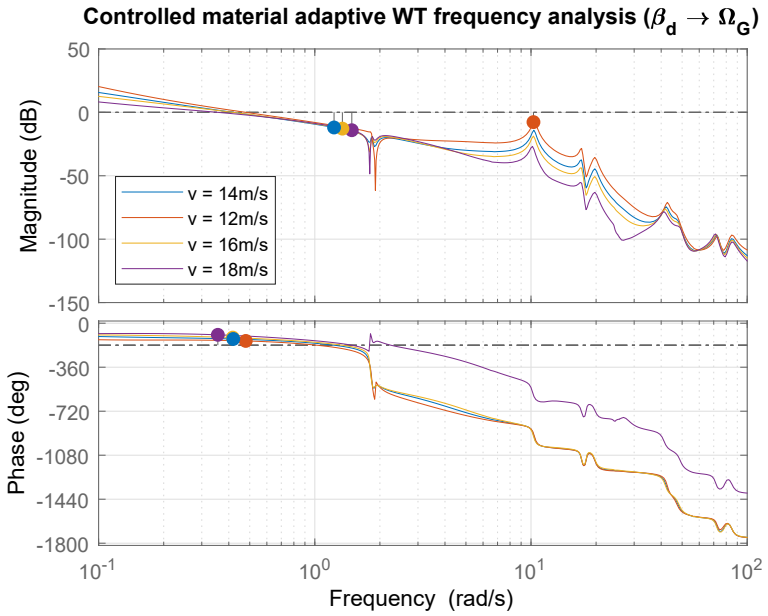

Figure 18: Combined adaptive 5 MW controlled wind turbine frequency response

Table 4: Combined adaptive 5 MW WT stability margins

v [m/s]	Gm [db]	Pm [deg]	Wpm [rad/s]	Delay Margin [s]
		Above rated controller		
12	7.68	35.1	0.479	1.28
14	11.9	51	**0.42**	2.12
16	12.8	62.4	0.417	2.61
20	14.1	85	0.356	4.17
		Below rated controller		
4	∞	55.3	**0.42**	2.3

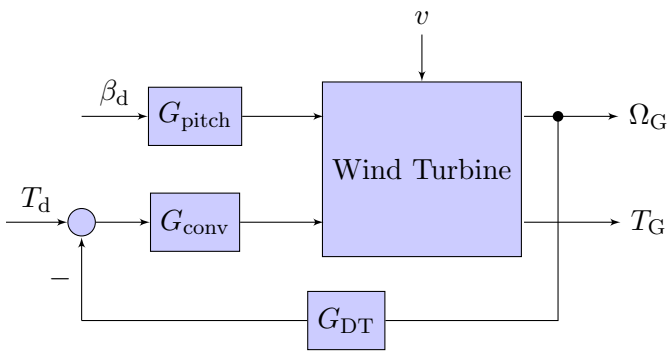

Figure 19: Feedback loop to increase drive-train damping

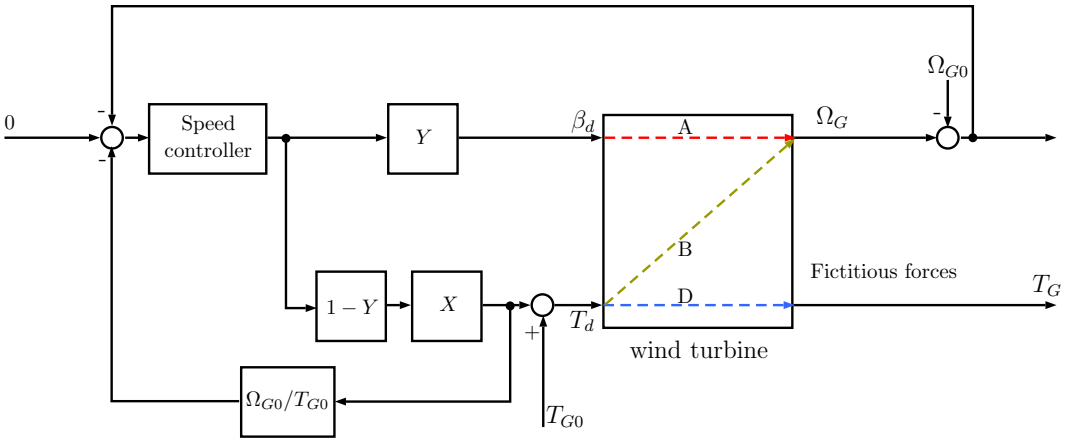

Figure 20: Power coordinated control scheme

4.3 Alleviation of fatigue loads in the drive-train

In order to reduce drive-train torque variations, the first drive-train mode is damped by feeding back generator speed measurement to torque demand as shown in Figure 19. A bandpass filter can be designed to increase damping at frequencies close to the drive-train resonant and to prevent the dynamics away from the drive-train frequency from being over-damped. The baseline, material adaptive and combined adaptive exemplar wind turbines have the same drive-train, thus the bandpass drive-train filter used is

$$G_{\mathrm{DT}}^{\mathrm{B,MA,CA}} = \frac{45674s}{2.5s^2 + 35s + 199.21} \tag{22}$$

4.4 Alleviation of fatigue loads in the tower

The right half plane zeroes arising from the interaction between the drive-train dynamics and the tower, at above rated wind speeds and at frequencies close to the tower frequency, can be removed by a control scheme called power coordinated control (PCC) [LS16], see Figure 20.

The control action of the PCC is achieved through a combination of pitch and torque demand. The element Y is designed as a low pass filter or a notch filter centred at the tower frequency to reduce pitch activity in the vicinity of such frequency. The element X is applied to torque demand such that the transmittance from its input to Ω_G is similar to the transmittance from β_d to Ω_G and thus the speed controller remains unchanged. For wind speeds, particularly just above rated, the generator speed obtained using PCC is the same as that using the speed

controller alone. However, there can be large power fluctuations because the gain from T_d to Ω_G is much weaker than that from β_d to Ω_G. These fluctuations have a direct impact on the drive-train components such as gearbox and generator [LS16]. A reduction in these fluctuations can be attained by replacing the speed control loop with a power control loop. Since the power converter is relatively fast acting, torque fluctuation (ΔT_G) about T_{G0} are relatively small compared to fluctuations $\Delta\Omega_G$ about Ω_{G0}, thus if P is well controlled then so is Ω_G and the power control loop from Figure 20 is similar to the speed control loop from Figure 8 at above rated wind speeds. The system output P can be expressed as

$$P \approx T_{G0}\left[\Omega_{G0} + (\Omega_G - \Omega_{G0}) + \frac{\Omega_{G0}}{T_{G0}}(T_G - T_{G0})\right] \tag{23}$$

with $P = \Omega_G T_G$. The element X is designed such that it counteracts the right half plane zeroes introduced by the interactions with the tower dynamics and stabilises the transmittance $\left(B + \frac{\Omega_{G0}}{T_{G0}}\right) A^{-1}$, while keeping the transmittance similarity

$$CA \approx CYA + C(1-Y)X(B+)\left(B + \frac{\Omega_{G0}}{T_{G0}}\right) \tag{24}$$

The transmittances A, B and D are transmittances from $(\beta_d \to \Omega_G)$, $(T_d \to \Omega_G)$ and $(T_d \to T_G)$, respectively. The element C represents the speed controller. A low order approximation suffices for X since only frequencies over a narrow range focused on the tower frequency are of interest.

The required control elements to implement PCC for the three 5 MW models are the following.

Baseline:

$$Y^{\mathrm{B}}(s) = \frac{s^2 + 0.3629s + 3.292}{s^2 + 2.903s + 3.292} \tag{25}$$

$$1 - Y^{\mathrm{B}}(s) = \frac{2.54s}{s^2 + 2.903s + 3.292} \tag{26}$$

$$X^{\mathrm{B}}(s) = \frac{-15173}{(s + 0.2032)(s + 1.8)(s + 12.9)(s + 535.3)} \tag{27}$$

Material adaptive:

$$Y^{\mathrm{MA}}(s) = \frac{s^2 + 0.3621s + 3.278}{s^2 + 2.897s + 3.278} \tag{28}$$

$$1 - Y^{\mathrm{MA}}(s) = \frac{2.535s}{s^2 + 2.897s + 3.278} \tag{29}$$

$$X^{\mathrm{MA}}(s) = \frac{-601.54}{(s + 0.2382)(s + 1.775)(s + 10.39)(s + 39.32)} \tag{30}$$

Combined adaptive:

$$Y^{\mathrm{CA}}(s) = \frac{s^2 + 0.3633s + 3.299}{s^2 + 2.906s + 3.299} \tag{31}$$

$$1 - Y^{\mathrm{CA}}(s) = \frac{2.543s}{s^2 + 2.906s + 3.299} \tag{32}$$

$$X^{\mathrm{CA}}(s) = \frac{-555.74}{(s + 0.1758)(s + 1.4)(s + 10.39)(s + 39.48)} \tag{33}$$

The developed controllers do not require further tuning when the PCC is implemented.

5 Simulation studies

Power production simulations are carried out for the three 5 MW exemplar wind turbines for mean wind speed values of (4, 6, 8, 10, 12, 14, 16, 18, 20, 22, 24) m/s; and with 10 % turbulence intensity. Demanded generator torque has been modified to account for the added drive-train losses. Simulated time series data is used to assess power capture, speed regulation, operation during gusts and fatigue loading on blades and tower.

5.1 Power capture

Figure 21 shows the power curve produced by the baseline model under steady-state conditions and the power curve obtained by applying the binning method on power production data from six different wind speed seeds. Output power data is grouped into wind speed bins so that an average output power is obtained for each bin. The size of a wind speed bin is 0.5 m/s as indicated in the IEC standard [IEC05]. Figures 22 and 23 show the same power curve comparison for the material adaptive and combined adaptive blade configurations, respectively. The binning method determines drifts in generated power, with respect to its steady-state counterpart, and the highest power standard deviation at below rated values. These drifts and standard deviation values correspond to the added drive-train losses and are similar for all three wind turbine exemplars, thus not affecting the assessment of the induced bend-twist coupling in the adaptive blade configurations. Power curve simulations also show that the generated power from the combined adaptive blade configuration is slightly higher, for any given below rated wind speed, see Figure 24. Such result is consistent with the results found in [SCL+17a].

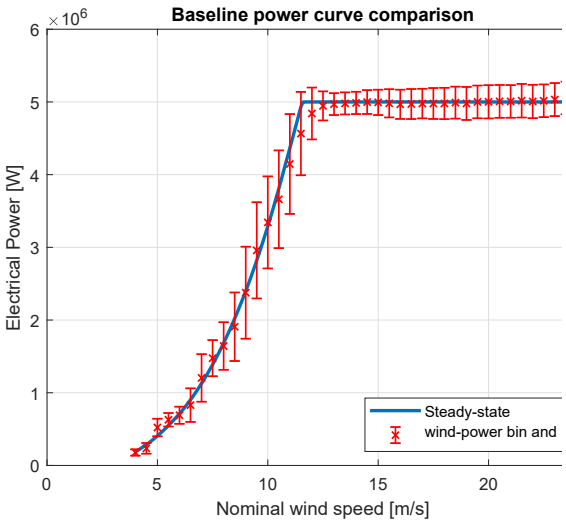

Figure 21: Baseline 5 MW WT generator power curve validation

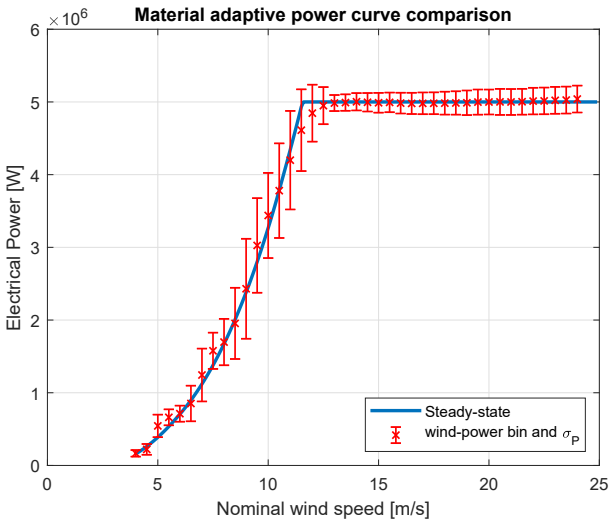

Figure 22: Material adaptive 5 MW WT generator power curve validation

5.2 Generator speed regulation

Controller design is first validated by comparing generator speed mean ($\mu_{\Omega_G,i}$) and standard deviation ($\sigma_{\Omega_G,i}$) and blade pitch rate standard deviation ($\sigma_{\beta,i}$) for three different wind speed seeds ($i = 1, 2, 3$) of the design wind speed of 14 m/s, see Table 5. At 14 m/s wind speed, the three developed controllers achieve the same crossover frequency and thus the system performance should be similar except for the effect caused by the induced bent-twist coupling. The

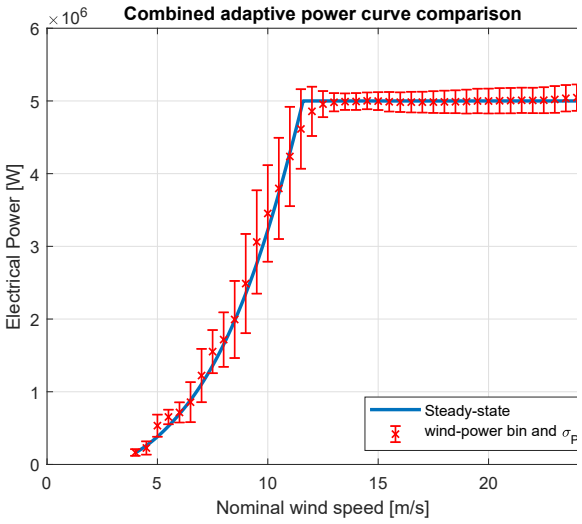

Figure 23: Combined adaptive 5 MW WT generator power curve validation

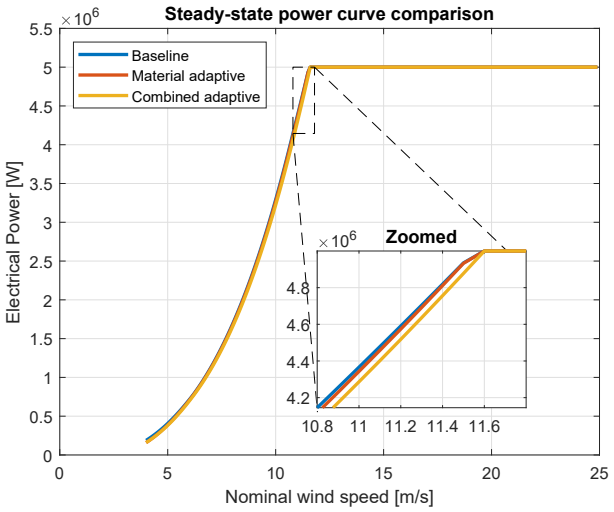

Figure 24: Power curve comparison: baseline, material and combined adaptive

statistics show that the lowest generator speed standard deviation is achieved by the combined adaptive blade configuration, followed by material adaptive and baseline model, respectively. However, the statistics for blade pitch rate shows that an increase in pitch activity is required to control both adaptive blade configurations. Increase activity in pitch and pitch rate for blade 2 can be seen in Figures 25 and 26, respectively. The increase is slightly higher in the material adaptive blade configuration. When comparing root bending moments, it can be seen that the two adaptive blade configurations present less blade structural loading, see Figure 27, and the material adaptive configuration presents the lowest tower nodding moment, see Figure 28, but such result will need to be verified using cycle counting.

Table 5: Mean and standard deviation values

	Baseline	Material Adaptive	Combined Adaptive
	Generator speed		
$\mu_{\Omega_G,1}[rad/s]$	123.1641	123.0673	123.0781
$\mu_{\Omega_G,3}[rad/s]$	123.0963	123.0294	123.0346
$\mu_{\Omega_G,6}[rad/s]$	123.0538	123.0050	123.0020
$\sigma_{\Omega_G,1}[rad/s]$	3.8162	2.6922	2.6702
$\sigma_{\Omega_G,3}[rad/s]$	3.6454	2.6528	2.6077
$\sigma_{\Omega_G,6}[rad/s]$	3.7505	2.6227	2.6170
	Blade pitch rate		
$\sigma_{\beta,1}$	0.0033	0.0042	0.0042
$\sigma_{\beta,3}$	0.0031	0.0042	0.0040
$\sigma_{\beta,6}$	0.0028	0.0038	0.0037

The performance of the developed controllers is also tested for (8, 12, 16) m/s wind speeds to cover below, rated and above rated scenarios, respectively. At below rated wind speed, particularly across the maximum power tracking region, the generator speed at which the adaptive blade configurations operate differ with that of the baseline model for the same wind speed magnitude. This variation is seen in Figure 29, for 8 m/s wind speed, where the average generator speed for the baseline model is 89.65 rad/s, whereas material adaptive and combined adaptive generator speeds are 96.94 rad/s and 96.82 rad/s, respectively. The power spectral density

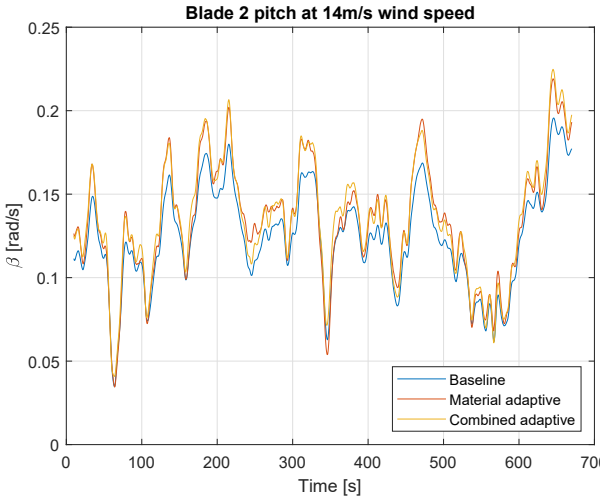

Figure 25: Blade pitch angle at 14 m/s wind speed

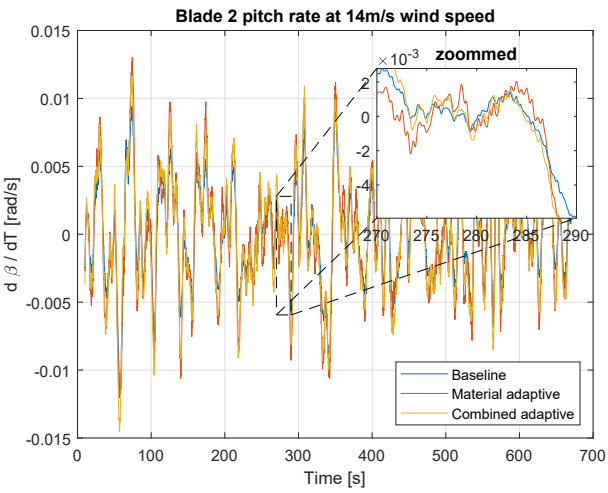

Figure 26: Blade pitch rate at 14 m/s wind speed

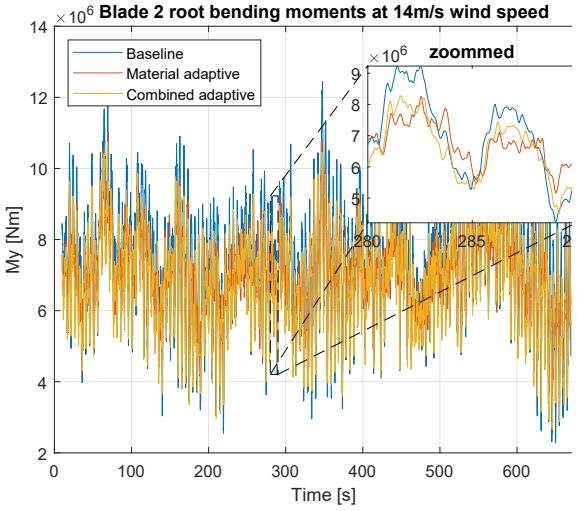

Figure 27: Blade in-plane root bending moment at 14 m/s wind speed

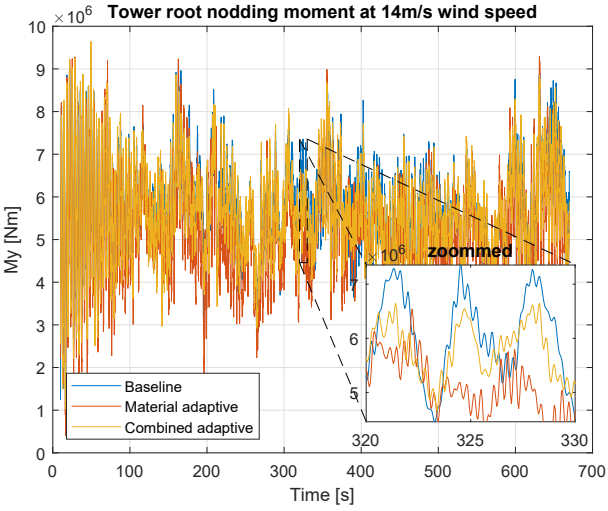

Figure 28: Tower root nodding moment at 14 m/s wind speed

(PSD) and the cumulative PSD of the three measured generator speed data is shown in Figure 30. The variation in generator speed is observed in the cumulative PSD where the baseline model presents the lowest magnitude, followed by material adaptive and combined adaptive respectively. At 12 m/s wind speed, the power content at low frequencies of the baseline generator speed is slightly higher than that of the adaptive blade configurations, see Figure 32. Material adaptive and combined adaptive PSD are fairly similar with some minor variations at mid frequency range which make material adaptive present the lowest cumulative PSD. Both adaptive configurations also show tighter generator speed regulation as seen in Figure 31. At 16 m/s wind speed the variation in energy content at low frequencies between the baseline model and the adaptive configurations is larger and some variation also appears at high frequencies, thus making both adaptive configurations achieve low cumulative PSD, see Figure 34. Generator speed regulations is tighter, see Figure 33, especially for the combined adaptive blade configuration since its controller reaches higher crossover frequencies at higher wind speed values, see Table 4. The tendency of combined adaptive cumulative PSD to decrease continues as wind

speed increases as seen in Figures 35 and 36.

Figure 29: Generator speed time series comparison at 8 m/s wind speed

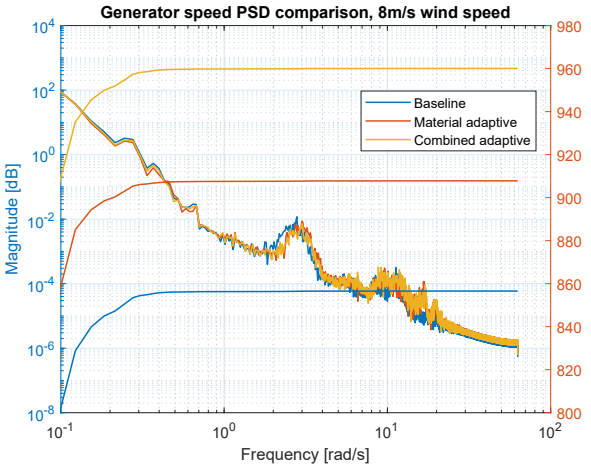

Figure 30: PSD and cumulative PSD comparison at 8 m/s wind speed

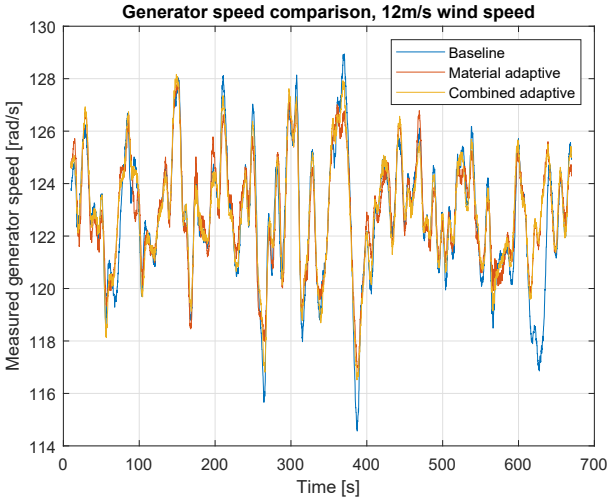

Figure 31: Generator speed time series comparison at 12 m/s wind speed

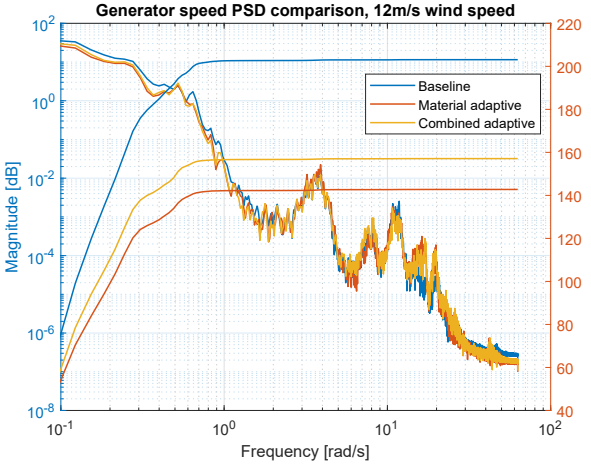

Figure 32: PSD and cumulative PSD comparison at 12 m/s wind speed

5.3 Operation during gusts

In gusty conditions, large pitch excursions are needed to keep constant power while the inertia of the blades limits the speed of the control system's response. Figure 37 shows a comparison of the three wind turbines generator speed during an operating gust scenario, at 14 m/s wind speed. Simulation results show that both adaptive blade configurations counteract the first portion of the Mexican hat-like gust without increasing blade pitch activity. At the highest peak value of the gust event, both adaptive configurations also reach peak blade pitch faster than the baseline model thus controlling generator speed quicker. Such controllability is maintained both during and after the gust event. Figure 38 shows a significant difference in blade pitch activity when wind speed goes roughly above 15 m/s. This difference is consistent with the comparison in steady-state pitch angle presented in Figure 15 since both adaptive configuration

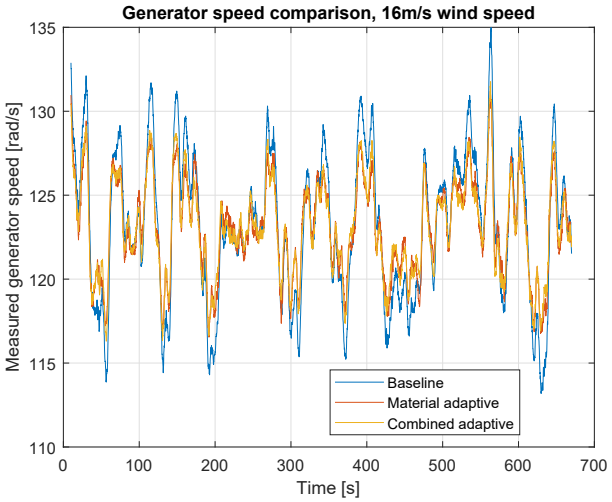

Figure 33: Generator speed time series comparison at 16 m/s wind speed

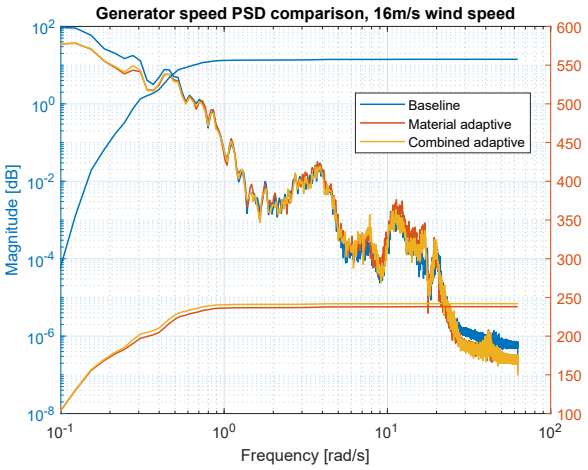

Figure 34: PSD and cumulative PSD comparison at 16 m/s wind speed

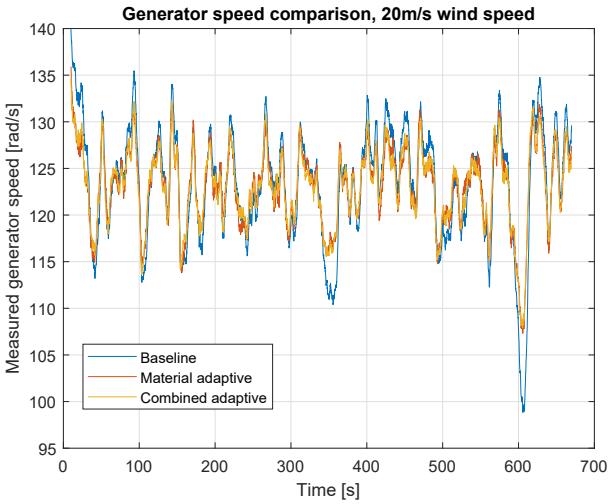

Figure 35: Generator speed time series comparison at 20 m/s wind speed

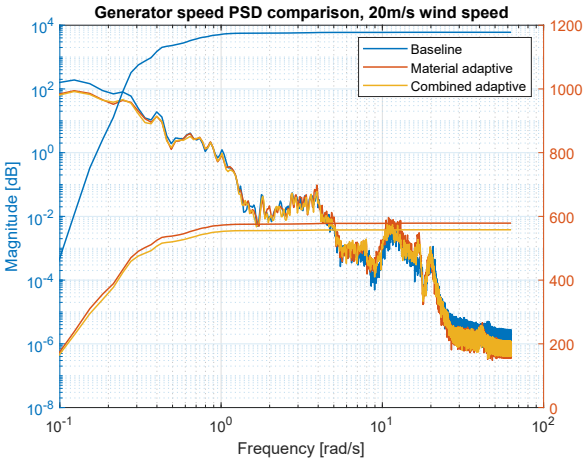

Figure 36: PSD and cumulative PSD comparison at 20 m/s wind speed

require higher pitch activity as wind speed increases to achieve a lower twist along the blade. Figure 39 corroborates such result as both adaptive configurations experience significantly less aerodynamic twist loading at the gust peak value which occurs at 213 s.

5.4 Fatigue analysis

The load alleviation capabilities of the three 5 MW exemplars wind turbines are compared by estimating damage equivalent loads (DELs). Key components to be considered are blades and tower, assessed at the root and base, respectively. Stress histories are used on the rainflow counting algorithm to estimate the DELs. DELs determine a single constant-rate fatigue load, which is material dependent and will produce equivalent damage [Sut99].

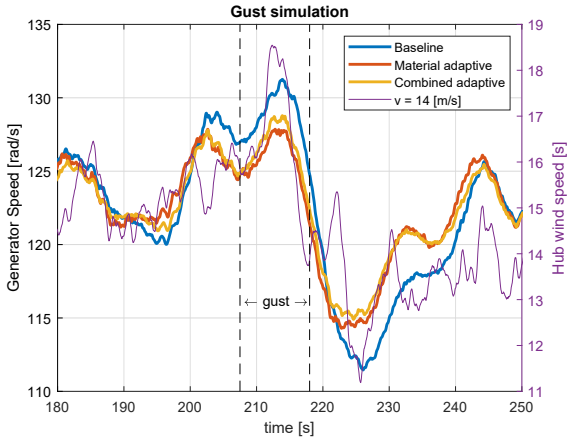

Figure 37: Generator speed comparison at 14m/s during gust

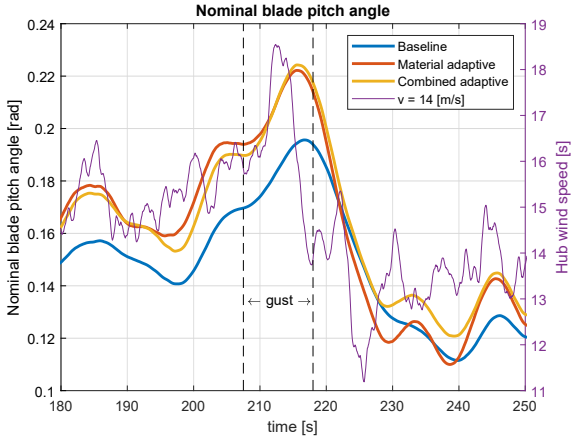

Figure 38: Blade pitch angle comparison at 14m/s during gust

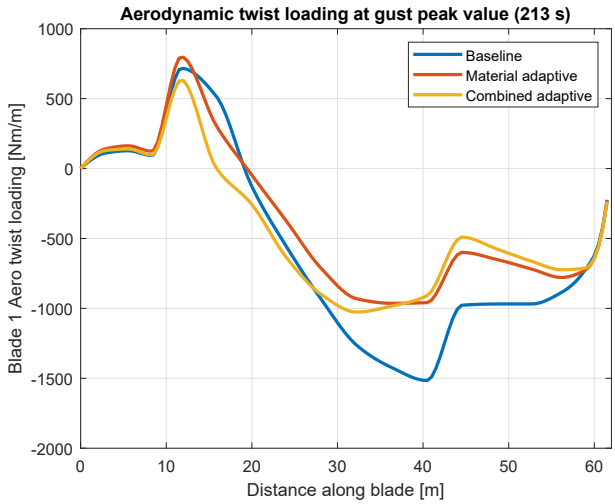

Figure 39: Blade 1 aerodynamic twist loading at gust peak value

DELs are given by

$$DEL = \left(\frac{\sum_i^k n_i L_i^m}{t_{\text{sim}f}} \right)^{\frac{1}{m}} \tag{34}$$

where n_i is the stress cycle at stress level σ_i, L_i is the amplitude of the cycle and m is the Wohler's exponent which is taken to be 3 for the turbine tower (welded steel) and 10 for the turbine blades (fiberglass composite) [JBM+09]. Constant t_{sim} is the duration of the original time history and f is the frequency at 1P. Stress loads histories are obtained from design load cases (DLC) 1.2 representing loads during power production over the operating wind speed range (4 m/s to 24 m/s). The annual wind speed distribution, determined by the Weibull distribution (8.5 m/s, $k = 2$), is used to calculate weighted DELs for given wind speeds, i.e.

$$DEL_{\text{weighted}} = \left(P\left(v\right) DEL^m \right)^{\frac{1}{m}} \tag{35}$$

where $P\left(v\right)$ is the wind speed probability calculated from the Weibull distribution. The total lifetime DELs are given by

$$DEL_{\text{lifetime}} = \left(\sum_{v=4}^{24} DEL_{\text{weighted}}^m \right)^{\frac{1}{m}} \tag{36}$$

Table 6: Equivalent fatigue loads

	Baseline	MA	CA
Tower M_{xy} lifetime EFL	1.1833E6	1.0615E6	1.0370E6
Blade M_x lifetime EFL	7.6789E5	8.1950E5	8.0532E5
Blade M_y lifetime EFL	5.2623E5	3.7938E5	4.2055E5
Blade M_{xy} lifetime EFL	5.7533E5	4.3879E5	4.7803E5

Weighted DEL estimates for blade 3 have been calculated for in-plane (M_x) and out-of-plane (M_y) root bending moments; and for blade and tower root twisting moments (M_{xy}). Both blade adaptive configurations show an increase in blade in-plane weighted DELs, see Figure 40. The lifetime equivalent fatigue loads shown in Table 6 show an increase of 6.7 % produced by the material adaptive configuration and an increase of 4.8 % produced by the combined adaptive configuration. Figure 41 shows that at below rated wind speeds the material adaptive configuration produces the highest increase in DELs whereas at high wind speeds the combined adaptive configuration produces the highest DELs increase. At speeds just above rated wind speed, both configuration produce a similar increase in DELs. Fatigue loads reduction is significant when out-of-plane DELs and twisting DELs are assessed. The material adaptive configuration achieves the highest reduction in out-of-plane weighted DELs, 27.9 % reduction in lifetime weighted DELs, compared to 20 % reduction produced by the combined adaptive configuration, see Figure 42. Figure 43 shows that DELs reduction produced by the material adaptive configuration is consistent throughout the operating envelope. Simulation results also show that at 6 m/s wind the combined adaptive configuration increases blade fatigue loads slightly. Material adaptive configuration also produces the highest twisting weighted DEL reduction, 23.7 %, compared with the reduction achieved by the combined adaptive configuration of 16.9 %, see Figure 44. Once again the reduction is consistent throughout the operating envelope. When assessing tower twisting weighted DELs, see Figure 46, the combined adaptive achieves a slightly higher reduction, 12.4 %, compared to the material adaptive configuration, 10.3 %. Figure 47 shows that combined adaptive achieves the highest reduction at above rated wind speeds without increasing fatigue loads at 6 m/s wind speed.

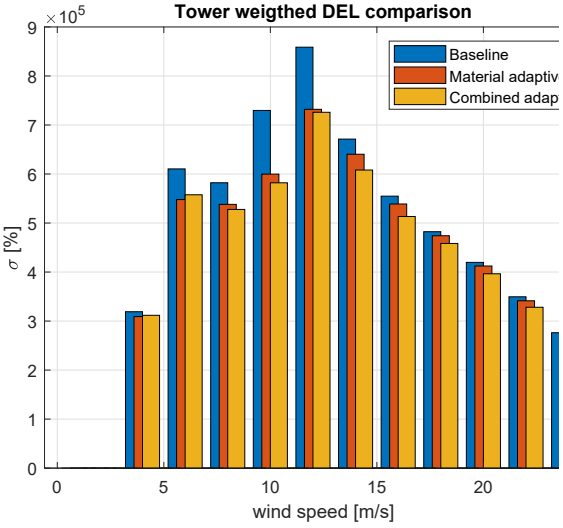

Figure 40: Blade root M_x weighted DEL comparison

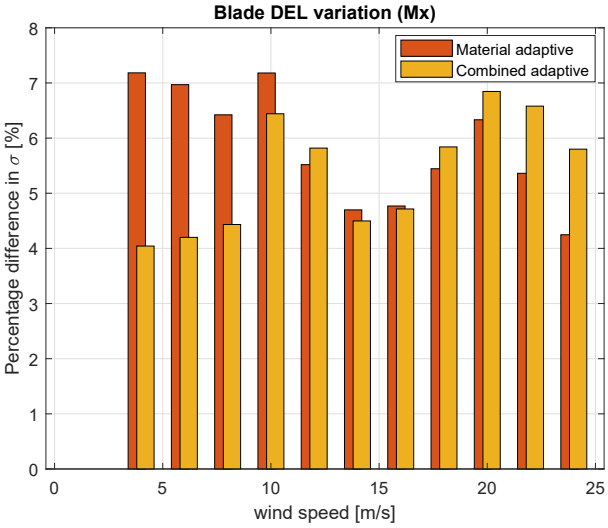

Figure 41: Blade root M_x DEL variation with respect to Baseline model

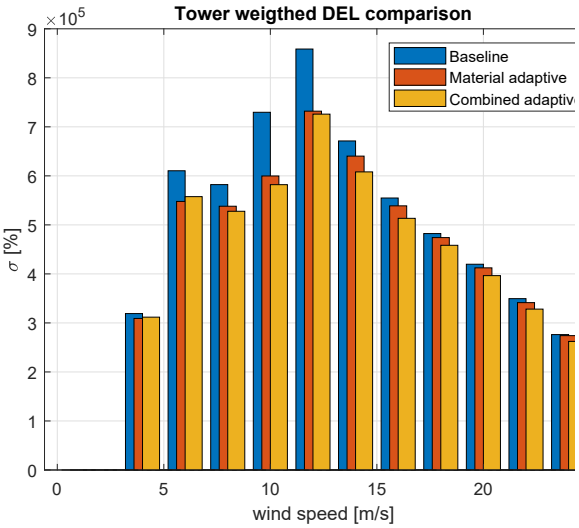

Figure 42: Blade root M_y weighted DEL comparison

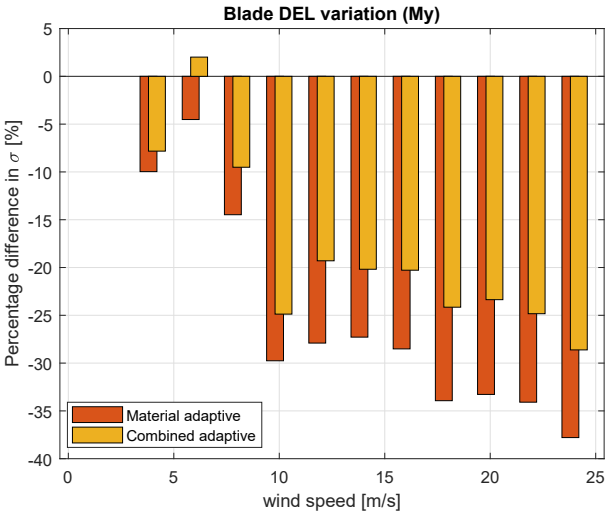

Figure 43: Blade root M_y DEL variation with respect to Baseline model

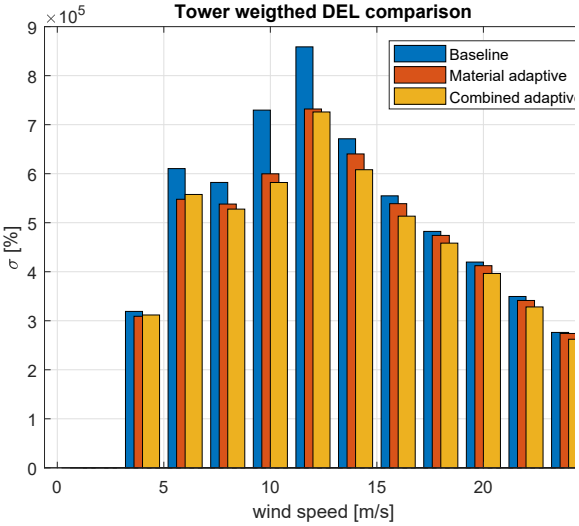

Figure 44: Blade root M_xy weighted DEL comparison

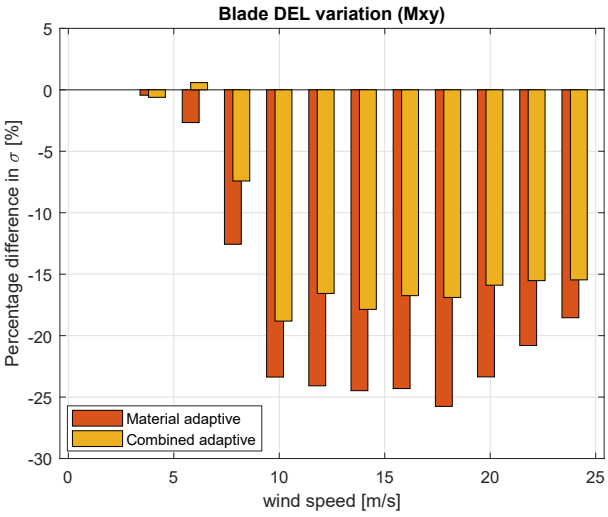

Figure 45: Blade root M_xy DEL variation with respect to Baseline model

6 DTU 10 MW Wind turbine control design and analysis

Controller design and turbine performance analysis of the DTU 10 MW wind turbine exemplar follows the same scheme presented in the controller design for the three 5 MW wind turbine exemplars. Blade aero-elastic twist response for different wind speeds is presented in Figure 48. The blade is designed to twist towards feather slightly throughout the operating envelope. At rated wind speed the blade tip achieves its highest twist which decreases as wind speed increases. At below rated wind speeds, the blade produces only a very small twist. The highest aerodynamic twist required by the turbines is exerted by the blade aerodynamic pre-twist and for a steady-state pitch is 3.88° at 12 m/s wind speed as seen in Figure 49.

Figure 50 shows a standard control strategy of the DTU 10 MW wind turbine in the torque/rotor speed plane. Tracking $C_{p_{\max}}$, makes the turbine overshoot rated torque and thus to enter the

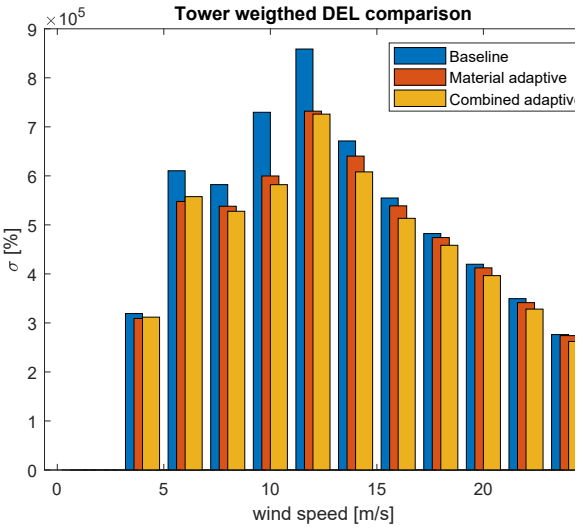

Figure 46: Tower base weighted DEL comparison

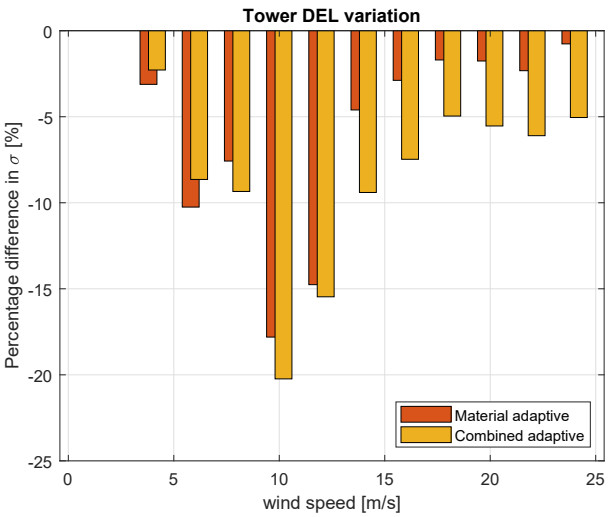

Figure 47: Tower base DEL variation with respect to Baseline WT exemplar

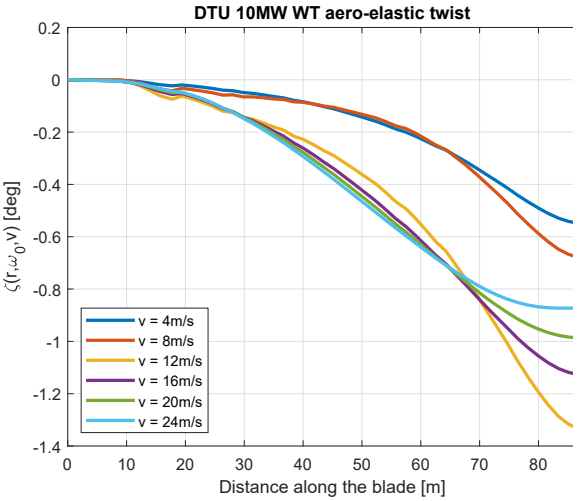

Figure 48: DTU 10 MW WT aero-elastic twist comparison

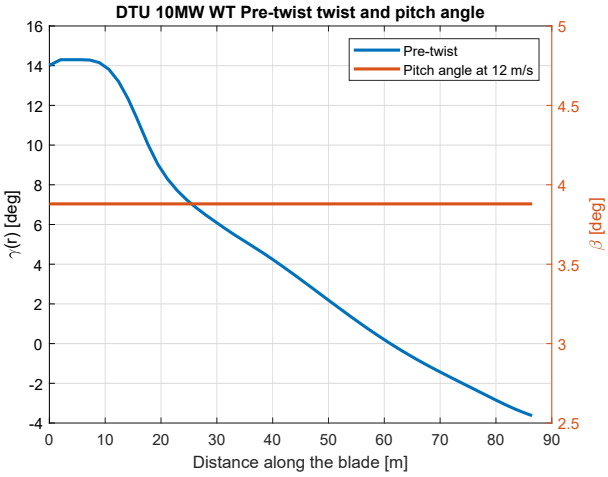

Figure 49: DTU 10 MW WT pre-twist and pitch angle

stall region before it reaches rated rotor speed. Off-setting $C_{p_{\max}}(\lambda^*, 0)$ reduces the value of K_{opt} thus allowing a very short speed region just before rated power is reached. This strategy is used in [MH13], see Figure 51, and results in reduced power capture across the variable speed region and undesirable switching transients between the variable speed region, the constant speed region and the above rated region due to the shortness of the second constant speed region. The second constant speed region can be elongated by allowing the turbine to pitch during the variable speed region, i.e. $C_{p_{\max}}(\lambda^*, 1)$ as shown in Figure 52. Energy capture is still reduced since the turbine is operating sub-optimally. A compromised can be achieved with a combination between $C_{p_{\max}}(\lambda^*, 0)$ tracking and below rated pitching as shown in Figure 53. At a set generator speed, just below rated value, the controller switches to a linear relationship between generator speed and torque to produce the pitch offset. Using this strategy more energy can be captured in below rated operation, increased size of the second constant speed region and reduced gain of the pitch controller.

The variation of $\frac{\partial T_f}{\partial \beta}$ with respect to β for the DTU 10 MW wind turbine is fairly linear as

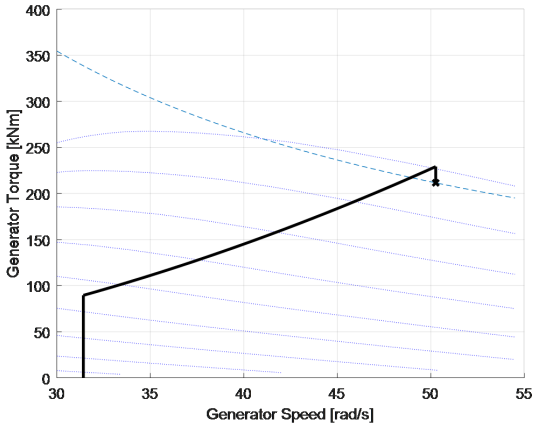

Figure 50: DTU 10 MW WT control strategy with $C_{p_{\max}}(\lambda^*, 0)$ tracking

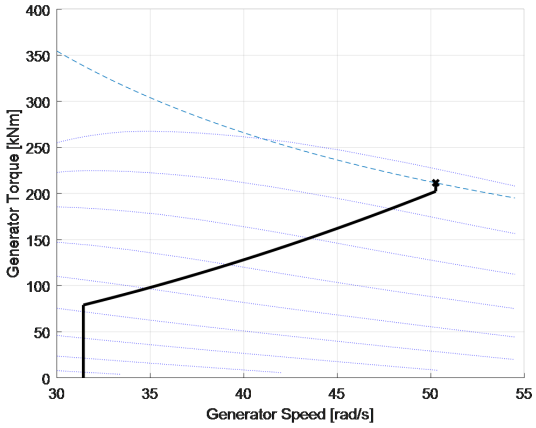

Figure 51: DTU 10 MW WT control strategy with off $C_{p_{\max}}(\lambda^*, 0)$ tracking

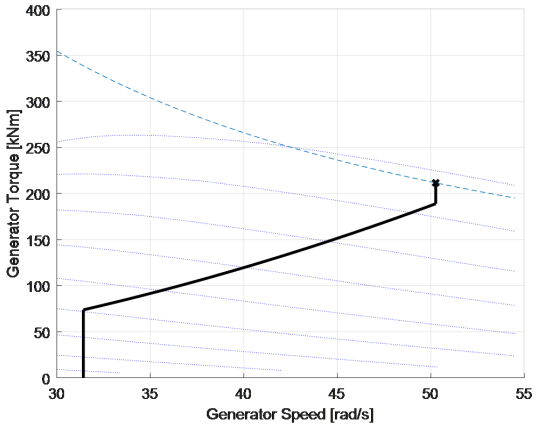

Figure 52: DTU 10 MW WT control strategy with constant below rated pitching $C_{p_{\max}}(\lambda^*, 1)$

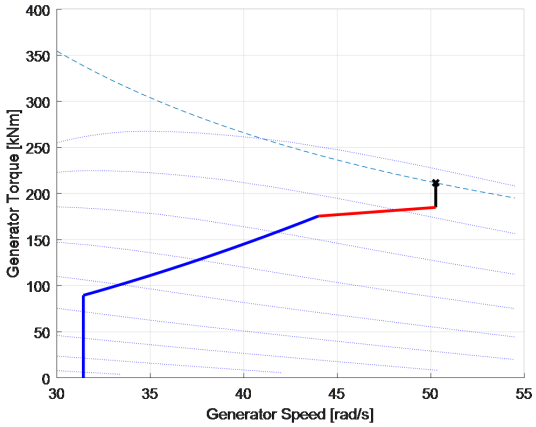

Figure 53: DTU 10 MW WT control strategy with $C_{p_{\max}}(\lambda^*, 1)$ tracking in a linear relationship

shown in Figure 54.

6.1 Control design for the DTU 10 MW wind turbine

The initial controller design follows the procedure used for the 5 MW wind turbine exemplars. The developed controllers are

$$C_{\text{br}}^{\text{DTU}}(s) = -\frac{168909\,(s + 0.1407)}{s\,(s + 1.923)} \tag{37}$$

$$C_{\text{ar}}^{\text{DTU}}(s) = -\frac{0.21\,(s + 0.1407)}{s\,(s + 1.923)} \tag{38}$$

$$K_{\text{gs}}^{\text{DTU}}(\beta) = \frac{1}{0.4\beta + 0.85} \tag{39}$$

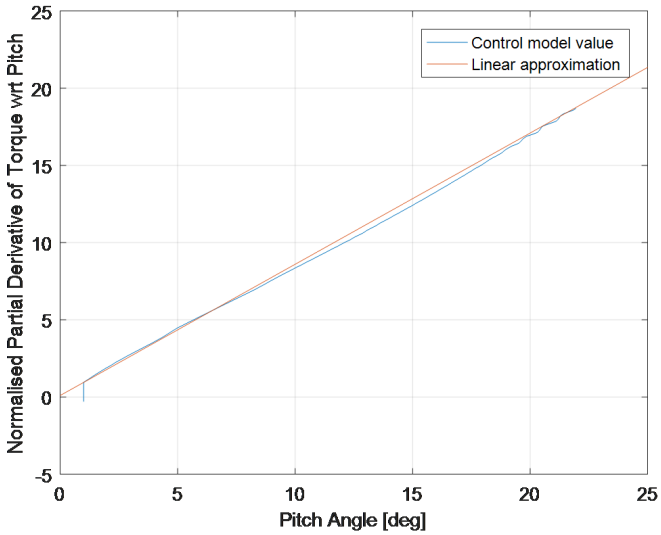

Figure 54: DTU 10 MW WT aerodynamic torque nonlinearity

$$K_{\text{opt}}^{\text{DTU}} = 90.7322 \tag{40}$$

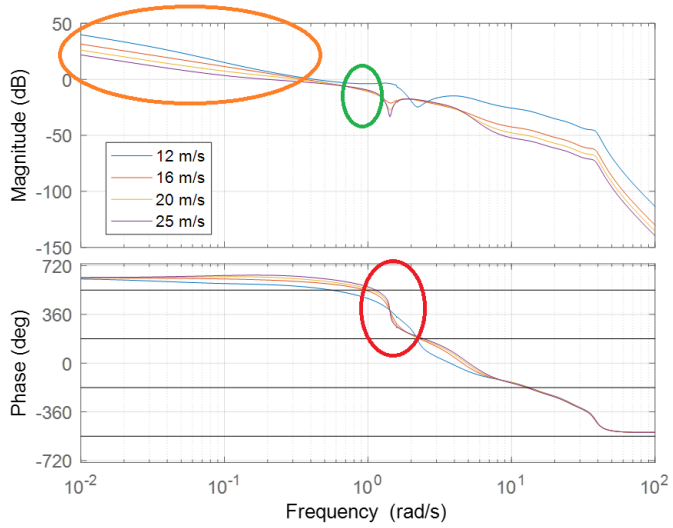

Figure 55: DTU 10 MW controlled wind turbine frequency response

Table 7: DTU 10 MW WT stability margins

v [m/s]	Gm [db]	Pm [deg]	Wpm [rad/s]
12	1.88	16.50	0.42
16	10.08	60.20	0.37
20	11.29	82.68	0.33
25	11.98	109.42	0.20

Frequency analysis can be seen in Figure 55. As shown in Table 7, the stability margins for the exemplar wind turbine are low even though the crossover frequency is reasonable. The

Table 8: Values of function $\psi_n(\beta_{di})$

	β_{d1}	β_{d2}	β_{d3}	β_{d4}
$\psi_1(\beta_d)$	α_{β_2}	α_{β_1}	α_{β_1}	α_{β_1}
$\psi_2(\beta_d)$	α_{β_3}	α_{β_3}	α_{β_2}	α_{β_2}
$\psi_3(\beta_d)$	α_{β_4}	α_{β_4}	α_{β_4}	α_{β_3}

baseline controller cannot achieve higher stability margins and so a new controller formulation is required. For larger wind turbines such as the DTU 10 MW wind turbine, in order to cater for low frequency variations of the dynamics of the linearised models about the locus of operating points, a nonlinear controller can be constructed by interpolating between linear controllers. Such controller should satisfy an extended local linear equivalence condition i.e. the linearisation, at any operating point, of the nonlinear controller should correspond to the associated member of the family of linear controllers [LL96]. The standard controller presented in Equation 8 is extended to satisfy this local linear equivalence condition by the following transfer function:

$$\frac{s+\alpha(\beta_d)}{s+k} \approx \frac{(s+\alpha_{\beta_{d1}})(s+\alpha_{\beta_{d2}})(s+\alpha_{\beta_{d3}})(s+\alpha_{\beta_{d4}})}{(s+k)(s+\psi_1(\beta_d))(s+\psi_2(\beta_d))(s+\psi_3(\beta_d))} \tag{41}$$

The resulting extended local linear equivalent controller or ELLE controller counteracts the varying low frequency pole, which dependents on $\frac{\partial T_f}{\partial \omega}$, with a zero $\alpha(\beta_d)$ scheduled with the operating points. $\psi_n(\beta_{di})$ for $n = 1, 2, 3$ and $i = 1, 2, 3, 4$ represent the zeros shown in Table 8. For convenience, k can be chosen to be equal to α_{β_1} such that at rated values the ELLE component is one.

Table 9: Value of ELLE poles and pitch angles

v [m/s]	$\alpha_{\beta_{di}}$	β_{di} [deg]
12	0.0536	1.45
15	0.1209	9.64
20	0.2989	16.52
25	0.5451	21.94

Since the dynamic behaviour of a nonlinear controller strongly depends upon the realisation adopted, all the nonlinear components of the ELLE controller must be placed after the main linear dynamics but immediately before the integral action. Detailed formulation of the ELLE controller can be found in [LL96] and its implementation on a 10 MW exemplar wind turbine in [Tho17]. The standard controller is split into an inner block and an outer block to account for smooth controller switching, that is

$$C_{\text{inner}} = -\frac{100N(s)}{s}$$
$$C_{\text{outer}} = \frac{K_c}{100D(s)}$$

The ELLE controller realisation will make the inner block improper since it contains the integral action and thus a pre-compensation is required. The pre-compensation required to implement the ELLE contoller on the DTU model is given by

$$G_{\text{pre}} = \frac{18s}{s^2 + 14.4s + 324} \tag{42}$$

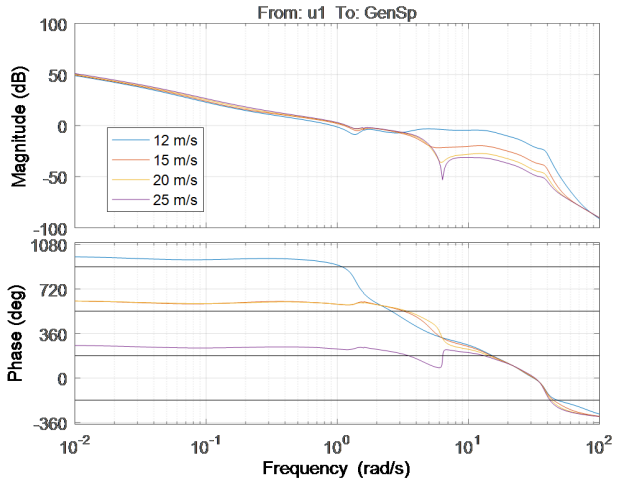

Figure 56: DTU 10 MW controlled wind turbine frequency response with ELLE controller

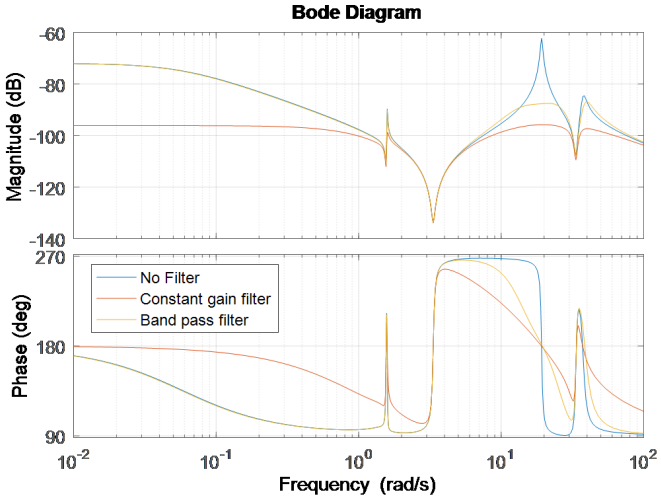

Figure 57: DTU torque demand to generator speed transmitance frequency analysis.

6.2 Alleviation of fatigue loads in the drive-train and the tower

The drive-train filter designed for the DTU 10 MW exemplar wind turbine is

$$G_{\mathrm{DT}}^{\mathrm{DTU}} = \frac{600000s}{s^2 + 26.32s + 353.4} \tag{43}$$

Bode plots of the dynamics from torque demand to generator speed are shown in Figure 57. A constant gain filter is also designed for comparison.

The required control elements to implement PCC on the DTU 10 MW model are the following.

$$Y^{\mathrm{DTU}}(s) = \frac{s^2 + 0.15s + 2.56}{s^2 + 0.45s + 2.56} \tag{44}$$

$$1 - Y^{\mathrm{DTU}}(s) = \frac{0.15s}{s^2 + 0.45s + 2.56} \tag{45}$$

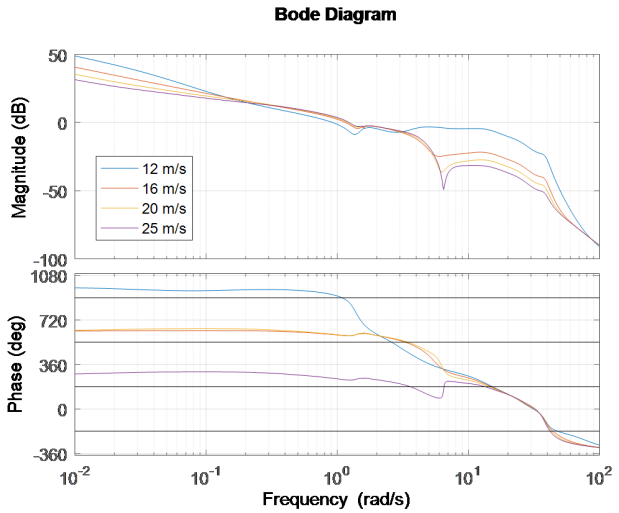

Figure 58: DTU 10 MW controlled wind turbine frequency response with retuned above rated controller

Table 10: DTU 10 MW WT stability margins for retuned above rated controller

v [m/s]	Gm [db]	Pm [deg]	Wpm [rad/s]
12	3.04	25.18	0.92
16	8.26	55.88	1.16
20	8.22	53.77	1.20
25	8.06	53.59	1.23

$$X^{\mathrm{DTU}}(s) = \frac{-1 \times 10^{7}(s+7)}{(s+10)^{3}(s+0.07)} \tag{46}$$

With the PCC control scheme the above rated controller needs to be re-tuned to

$$C_{\mathrm{ar}}^{\mathrm{DTU}}(s) = -\frac{0.2415(s+0.1407)}{s(s+1.923)} \tag{47}$$

The new controller design achieves a better trade-off between stability and bandwidth as seen in Table 10. The frequency analysis with the retuned controller is presented in Figure 58.

6.3 Simulation results

The steady-state power curve for the DTU 10 MW wind turbine can be seen in Figure 59. The use of the ELLE controller produces a clear improvement in the standard deviation of the rotor speed at above rated wind speeds, as seen as percentage improvement in Figure 60. Smoother speed regulation produces an increase in pitch activity which leads to an increase in fatigue loading in the tower. Assuming a class I site as defined in the IEC standards, the comparison of the DELs produced by using the basic controller to those produced with the ELLE shows that there is an increase in the tower fore-afft DELs of 1.79%. Such increment is undesirable but the combination ELLE + PCC can achieve a further decrease of 0.55% in tower DELs at the expense of increase in rotor speed standard deviation as seen in Figure 61. Using the re-tuned controller from Equation 47, the tower DELs increase can be restricted to be 0.47%, with as much as 21% decrease in rotor speed standard deviation.

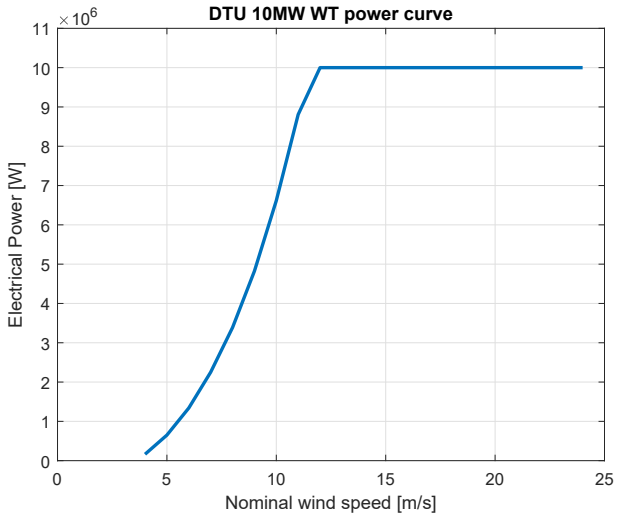

Figure 59: DTU 10 MW WT power curve

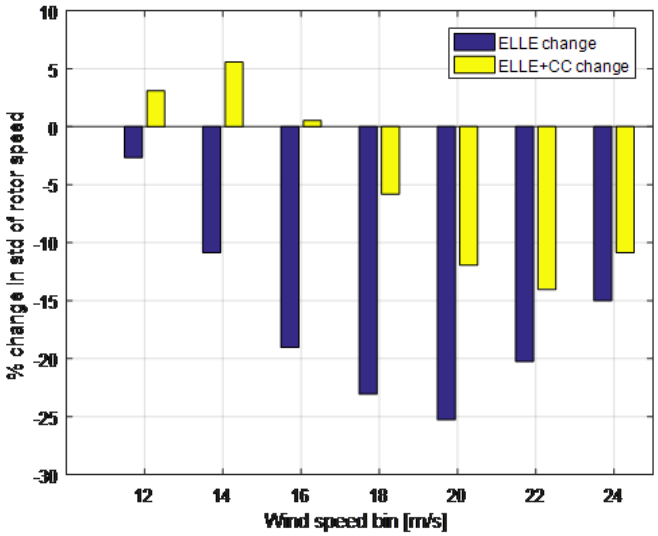

Figure 60: Change in standard deviation (STD) of rotor speed with ELLE and with ELLE pluss CC compared to basic control

7 Conclusions

Control systems to regulate generator speed and reduce fatigue loads have been designed for three 5 MW wind turbines, NREL baseline, material adaptive blade configuration and combined adaptive blade configuration; and for the DTU 10 MW exemplar wind turbine.

Regarding the 5 MW wind turbines, both blade adaptive configurations induce aerolastic twist towards feather to promote loads alleviation. Basic control systems are designed for each exemplar wind turbine at 14 m/s wind speed. The controllers are designed in a way they all achieve the same crossover frequency of 0.42 rad/s with almost the same controller dynamics thus removing the effect of the controllers in the performance of the wind turbines and allowing the assessment of the induce BTC of the adaptive configurations. Power coordinated control (PCC) is added to the full envelope controller to aid fatigue loads reduction, beyond of what the adaptive blade configurations can attain. Drive-train efficiency is also modified to allow the operating strategies to be comparable to some extent. Simulation results show that the con-

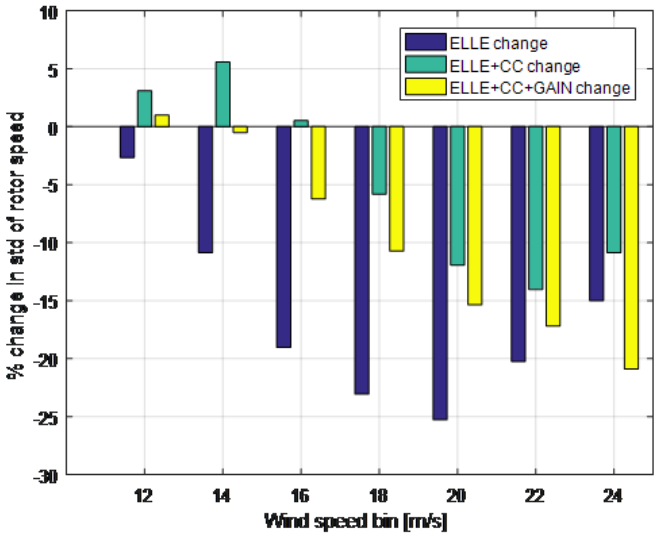

Figure 61: Change in standard deviation (STD) of rotor speed with ELLE, ELLE pluss CC and ELLE plus CC with an increase to the controller gain, all compared to basic control

trollability of both adaptive configurations is improved even though the close-loop achievable bandwidth is the same for the three turbines, at design wind speed. At other wind speeds the combined adaptive configuration is the best performing turbine and PSD analysis in generator speed data shows that its efficiency improves as wind speed increases. PSD analysis also shows that the material adaptive configuration performs better at low wind speeds which suggest that, at wind speeds below or near rated wind speed, the combined adaptive configuration requires a tighter control action. On gust simulations, both adaptive configurations achieve a better regulation and a significant reduction in aerodynamic twist loading, particularly from mid to tip blade span. Steady-state power curves do not show increase in power generation. Power production may differ if the original drive-train efficiencies are used but those studies are not carried out in this report since variation in drive-train efficiency is required to obtain a fair comparison of the developed controllers. Finally when DELs are compared, in-plane DELs show that both adaptive configuration increase blade loading by around 5 %, compared to the baseline model. Nonetheless, significant reductions in blade loading is shown in out-of-plane DELs and twisting DELs as well as in tower twisting loadings, thus confirming the benefits of induced BTC on blade configurations as reported in [SCL$^+$17a]. It is worth mentioning that the combined adaptive configuration seems to increase blade loadings at below rated wind speed but this can be due to the change in drive-train efficiency as both configurations were design with a higher drive-train efficiency.

Regarding the DTU 10 MW wind turbine, a linearised model is obtained to aid controller design. The aerodynamic behaviour of this turbine does not allow control strategies with conventional maximum power tracking, instead below rated pitch is introduced to achieve a sub-optimal turbine operation. The wind turbine further requires the extended local linear equivalence (ELLE) controller to improve speed tracking at above rated wind conditions. Tighter speed control leads to increase in pitch activity and consequently increase in tower fatigue loads. A trade-off between smooth control and reduction of tower DELs is attained by a re-tuned basic controller, the ELLE component and the PCC. Such approach is an active control solution, thus not requiring any alterations of the design of the tower.

References

[CM92] D C Corbet and C A Morgan. Report on the passive control of horizontal axis wind turbines. *ETSU WN*, 6043, 1992.

[CPW14] M Capuzzi, A Pirrera, and P M Weaver. A novel adaptive blade concept for large-scale wind turbines. Part II: Structural design and power performance. *Energy*, 73:25–32, 2014.

[CPW15] M Capuzzi, A Pirrera, and P M Weaver. Structural design of a novel aeroelastically tailored wind turbine blade. *Thin-Walled Structures*, 95:7–15, 2015.

[IEC05] International Electrotechnical Comission IEC. IEC 61400-12-1 Power performance measurements of electricity producing wind turbines. Technical report, 2005.

[JBM+09] J Jonkman, S Butterfield, W Musial, G Scott, J Jonkman, S Butterfield, W Musial, and G Scott. Definition of a 5-MW Reference Wind Turbine for Offshore System Development Definition of a 5-MW Reference Wind Turbine for Offshore System Development. Technical Report February, National Renewable Energy Laboratory, Colorado, 2009.

[LC00] W E Leithead and B Connor. Control of variable speed wind turbines : Design task. *International Journal of Control*, 73(13):1189–1212, 2000.

[LH02] James Locke and Ivan Contreras Hidalgo. *The implementation of braided composite materials in the design of a bend-twist coupled blade*. Sandia National Laboratories, 2002.

[LL96] W E Leithead and D J Leith. APPROPRIATE REALISATION OF GAIN-SCHEDULED CONTROLLERS WITH APPLICATION TO WIND TURBINE REGULATION. *International Journal of Control*, 65(4):555–572, 1996.

[LS16] William Leithead and Adam Stock. *Wind turbine control*, pages 219–258. Routledge, United Kingdom, 8 2016.

[LV03] Don W Lobitz and Paul S Veers. Load Mitigation with Bending/Twist-coupled Blades on Rotors using Modern Control Strategies. *Wind Energy*, 6(2):105–117, 2003.

[LVE+01] Don W Lobitz, Paul S Veers, G Richard Eisler, David J Laino, Paul G Migliore, and Gunjit Bir. The use of twist-coupled blades to enhance the performance of horizontal axis wind turbines. *SAND2001-1003, Sandia National Laboratories, Albuquerque, NM*, 2001.

[LVI03] James Locke, Ulyses Valencia, and Kosuke Ishikawa. Design studies for twist-coupled wind turbine blades. In *ASME 2003 Wind Energy Symposium*, pages 324–331. American Society of Mechanical Engineers, 2003.

[LVL99] Don W Lobitz, Paul S Veers, and David J Laino. Performance of twist-coupled blades on variable speed rotors. Technical report, Sandia National Labs., Albuquerque, NM (US); Sandia National Labs., Livermore, CA (US), 1999.

[MH13] Hansen Morten Hartvig and Lars Christian Henriksen. Basic DTU Wind Energy controller Department of Wind Energy Report 2013. Technical report, 2013.

[SCL+17a] Samuel Scott, Marco Capuzzi, David Langston, Ervin Bossanyi, Graeme McCann, Paul M Weaver, and Alberto Pirrera. Effects of aeroelastic tailoring on performance characteristics of wind turbine systems. *Renewable Energy*, 114:887–903, 2017.

[SCL+17b] Samuel Scott, Marco Capuzzi, David Langston, Ervin Bossanyi, Graeme McCann, Paul M. Weaver, and Alberto Pirrera. Effects of aeroelastic tailoring on performance characteristics of wind turbine systems. *Renewable Energy*, 114:887–903, 2017.

[Sut99] H. J. Sutherland. On the Fatigue Analysis of Wind Turbines. Technical report, Sandia National Laboratories, Albuquerque, 1999.

[Tho17] David William Thompson. *Mitigating Size Related Limitations in Wind Turbine Control*. Phd, Strathclyde University, 2017.

8 Appendix

8.1 Wind turbine parameters to construct linearised models

The following variables, shown in Table 11, are required to construct a linearised model of the three 5 MW wind turbine exemplars and the DTU 10 MW exemplar. Drive-train efficiency and nominal generator torque have been modified to allow to some extent a fair comparison of the control strategy.

Table 11: Variables for linearised model

Variable	Wind Turbines			
	5 MW	5 MW MA	5 MW CA	10 MW
Tower Fore-Aft Frequency $[rad/s]$	1.814	1.797	1.803	1.6
Tower Fore-Aft Damping $\left[Nms^2/rad^2\right]$	0.01	0.01	0.01	0.005
Tower Side to Side Frequency $[rad/s]$	1.803	1.797	1.803	1.587
Tower Side to Side Damping $\left[Nms^2/rad^2\right]$	0.01	0.01	0.01	0.005
Tower Shape factor	2	2	2	2
Hub Inertia $\left[kgm^2\right]$	115926	115926	115926	325671
Low speed Shaft Damping $[Nms/rad]$				250000
High Speed Shaft Damping $[Nms/rad]$				100
Low Speed Shaft Stiffness $[Nm/rad]$	8.68E+08	8.68E+08	8.68E+08	2.45E+09
High Speed Shaft Stiffness $[Nm/rad]$				9.812E9
Low Speed Shaft Material Damping $[Nms/rad]$				9.241E6
High Speed Shaft Material Damping $[Nms/rad]$				3696.4
Gearbox Ratio	97	97	97	50
Compound Inertia of the Gearbox $\left[kgm^2\right]$				70
High Speed Shaft Inertia $\left[kgm^2\right]$	0	0	0	1.00E-08
Generator Inertia $\left[kgm^2\right]$	534.116	534.116	534.116	1500.5
Drive-train Efficiency Below Rated	**0.90**	**0.90**	**0.90**	0.94
Drive-train Efficiency Above Rated	**0.90**	**0.90**	**0.90**	0.94
Rotor Radius $[m]$	63.13	63.13	63.13	89.17
Effective Blade Length $[m]$	44.19	44.19	44.19	62.42
Centre of Mass of Equivalent Blade $[m]$	20.6	21.58	21.93	26.13
Blade Mass $[kg]$	16762	17138	16344	41741
Flap Natural Frequency (Rotating) $[rad/s]$				
Flap Natural Frequency (Static) $[rad/s]$	4.42	3.93	3.77	3.87
Edge Natural Frequency (Rotating) $[rad/s]$				
Edge Natural Frequency (Static) $[rad/s]$	7.05	6.58	6.61	5.9
Edgewise Material Damping $[Nms/rad]$	0.01	0.01	0.01	0.004
Flapwise Material Damping $[Nms/rad]$	0.01	0.01	0.01	0.004
Rotor Inertia $\left[kgm^2\right]$	36746750	39893020	39174260	1.57E+08
Rotor-Hub factor [%]				
Hub Height $[m]$	90	90	90	118.88
Rotor and Nacelle Mass $[kg]$	347066	348193	345811	676968
Minimum Generator Speed $[rad/s]$	70.1624	70.1624	70.1624	31.416
Maximum Generator Speed $[rad/s]$	122.909864	122.909864	122.909864	50.2656
Cut In Wind Speed $[m/s]$	4	4	4	4
Cut Out Wind Speed $[m/s]$	25	25	25	25
Nominal Generator Torque $[Nm]$	**45200**	**45200**	**45200**	211642
Fine Pitch Angle $[deg]$	0	0	0	1
Feather Pitch Angle $[deg]$	90	90	90	90
Pitch Actuator	$\frac{39.48}{s^2+8.79s+39.48}$	$\frac{39.48}{s^2+8.79s+39.48}$	$\frac{39.48}{s^2+8.79s+39.48}$	$\frac{32.49}{s^2+7.98s+32.49}$